Article:

Craig, TJ orcid.org/0000-0003-2198-9172, Jackson, JA, Priestley, K et al. (1 more author) (2011) Earthquake distribution patterns in Africa: their relationship to variations in lithospheric and geological structure, and their rheological implications. Geophysical Journal International, 185 (1). pp. 403-434. ISSN 0956-540X

https://doi.org/10.1111/j.1365-246X.2011.04950.x

Earthquake distribution patterns in Africa: Their relationship to variations in lithospheric and geological structure, and their rheological implications

T. J. Craig, J. A. Jackson, K. Priestley, D. McKenzie
Bullard Laboratories, Department of Earth Sciences,
University of Cambridge, Cambridge, CB3 0EZ, UK
Email: tjc52@esc.cam.ac.uk

January 10, 2011

Abstract

We use teleseismic waveform inversion, along with depth phase analysis, to constrain the centroid depths and source parameters of large African earthquakes. The majority of seismic activity is concentrated along the East African rift system, with additional active regions along stretches of the continental margins in north and east Africa, and in the Congo basin. We examine variations in the seismogenic thickness across Africa, based on a total of 227 well determined earthquake depths, 112 of which are new to this study. Seismogenic thickness varies in correspondence with lithospheric thickness, as determined from surface-wave tomography, with regions of thick lithosphere being associated with seismogenic thicknesses of up to 40 km. In regions of thin lithosphere, the seismogenic thickness is typically limited to ≤20 km. Larger seismogenic thicknesses also correlate with regions that have dominant tectonothermal ages of ≥1500 Ma, where the East African rift passes around the Archean cratons of Africa, through the older Proterozoic mobile belts. These correlations are likely to be related to the production, affected by method and age of basement formation, and preservation, affected by lithospheric thickness, of a strong, anhydrous lower crust. The Congo basin contains the only compressional earthquakes in the continental interior. Simple modelling of the forces induced by convective support of the

African plate, based on long-wavelength free-air gravity anomalies, indicates that epeirogenic effects are sufficient to account for the localisation and occurrence of both extensional and compressional deformation in Africa. Seismicity along the margins of Africa reflects a mixture between oceanic and continental seismogenic characteristics, with earthquakes in places extending to 40 km depth.

Keywords

Earthquake source observations; Seismicity and tectonics; Dynamics: gravity and tectonics; Africa.

1 Introduction

The view has long been held that seismicity within the continental lithosphere indicated a generic strength profile consisting of a strong, seismogenic upper crust, a weak, aseismic lower crust, and a strong, occasionally seismogenic, uppermost mantle (e.g., Chen and Molnar 1983). However, reassessments of the global distribution of earthquake depths (Maggi et al., 2000) and of the techniques used in determining effective elastic thicknesses (McKenzie and Fairhead, 1997) have demonstrated that improved, more recent observations required a revision of this existing model. A series of studies, drawing on observations spanning seismology, gravity, metamorphic petrology, rock mechanics, heat flow and thermal modelling has led to a new model for the global seismicity within the lithosphere, summarised by Jackson et al. (2008).

In this revised model, seismicity in both the oceanic and continental mantle is limited to regions colder than $\sim 600°$C. In the oceans, where Moho temperatures away from oceanic ridges are $<600°$C, seismic activity is everywhere confined to a single layer, continuous from the top of the crust down to the $600°$C isotherm, a depth that is dependent on the age and cooling history of the oceanic plate (McKenzie et al., 2005).

In the continents, Moho temperatures are typically at $> 600°C$, leading to the continental mantle being generally aseismic. Maggi et al. (2000) hence concluded that continental seismicity is typically confined to the crust, as a single strong layer. In the majority of continental regions, this is limited to the upper crust, and corresponds to temperatures $<\sim 350°C$. However, in some regions — often associated with the ancient cratons — the seismogenic layer includes the whole of the crust, and must include earthquakes in material at temperatures of $350 – 600°C$ (McKenzie et al., 2005).

There are likely two factors behind these two behaviours. Firstly, cratonic regions are often associated with a thick, low-density lithospheric mantle root, which provides a degree of thermal insulation from the underlying convective mantle, making the crust relatively cold. The second factor is that the composition of the lower crust in such areas is likely to have a bulk mineral assemblage similar to dry granulite-facies material, which retains sufficient strength to be seismogenic at much higher temperatures than that of other crustal material, due to its anhydrous composition (Rudnick and Fountain, 1995; Lund et al., 2004). This effect is ultimately one of homologous temperature (the ratio of temperature to melting temperature), which determines the onset of high-temperature creep in most materials. The homologous temperature that limits mantle seismicity to $< 600°C$ is similar to that limiting seismicity to $< 350°C$ in a wet, quartz dominated upper crust, and to $< 600°C$ in dry granulite-facies rocks.

Modelling of the geotherm in areas with this increased seismogenic thickness, taking account for the presence of a mantle root, indicates that the cooling effect of a thick underlying lithosphere is insufficient to alone account for the depth of these lower crustal earthquakes (McKenzie et al., 2005). This implies that there is likely a compositional difference, and related change in absolute melting temperature, controlling the first-order depth of the seismic-aseismic transition in continental crust, with the temperature-dependent rheological behaviour of a given composition defining the precise depth of the transition.

This study is concerned with the seismicity of Africa (Figure 1), and how it relates to this emerging model for continental seismicity. Given the range of tectonic regimes present in Africa, extending across regions with such a long and varied geological history, ranging from Archean to present, the African continent also represents an excellent opportunity for investigating the controls exerted on the distribution and localisation of active deformation within a continental setting by pre-existing structure in the crust and upper mantle. We further consider the evidence for these controls that is preserved in the basement history of Africa, and how the spatial variation in deformation reflects the large-scale geodynamics of the continent.

The majority of Africa amalgamated in the Late Precambrian, and has remained as a cohesive unit ever since. The tectonic architecture of the continent is based around several stable Archean cratonic nuclei, separated and surrounded by younger Proterozoic mobile belts, many of which are associated with the Late Neoproterozoic Pan-African tectonothermal event (Meert, 2003; Begg et al., 2009). Following assembly as part of the Gondwana supercontinent, Africa has been affected only by minor phases of internal extension concurrent with rifting along its eastern and western margins, and by the formation of the orogenic Cape Fold Belt at its southern tip, until the Cenozoic. In contrast to its stability though much of the Phanerozoic, present day Africa displays a range of deformation from compression and orogenesis in NW Africa, compression across the Congo basin, continental rifting along the East African rift system (EARS hereafter), to the transition from continental rifting to active oceanic spreading in Afar, the Red Sea and the Gulf of Aden. The combination of an old stable basement, preserving a complex collisional history, and numerous types of active deformation allow investigation into the controls exerted by crustal and upper mantle structure on deformation within the continent.

Previous studies of seismicity in Africa (e.g., Chen and Molnar 1983; Shudofsky et al. 1987; Nyblade et al. 1996a; Foster and Jackson 1998; Yang and Chen 2010) identified the presence of deep, lower-crustal earthquakes within parts of the EARS, down to $\sim$35 km. This contrasts with most other areas of active continental rifting (e.g., Greece, western USA, western Turkey), where seismicity is limited to ∼15 km depth within the upper crust, in agreement with the $\sim 350°$C thermal constraint (Jackson and White, 1989; M[c]Kenzie et al., 2005). Notably, these deep crustal earthquakes occur only in the southern and western parts of the rift associated with proximity to the Archean cratons, suggesting a compositional and thermal control on their occurrence along the rift (Figure 1). In other continental regions, lower crustal seismicity has been linked to increased effective elastic thickness (T_e), as determined from studies of the admittance or coherence between gravity and topography (Hartley et al., 1966; Pérez-Gussinyé et al., 2009). However, such techniques for determining T_e lack the spatial resolution possible from studies of the seismic activity. Additionally, they are not appropriate for use in Africa, due to the large effects of dynamic support of the topography, and the probability of significant internal loading without topographic expression, in a continent that has remained stable on such a long timescale (M[c]Kenzie, 2003, 2010). None the less, the association of lower-crustal earthquakes with lithosphere that is relatively strong is probable (Maggi et al., 2000), and best demonstrated in the forelands of mountain belts (Jackson et al., 2008).

We begin by considering the seismicity along the extensional Gulf of Aden-Red Sea system, and then investigate the seismic activity along the EARS. We then study the seismic activity along the margins of East Africa, Egypt, and Morocco/Algeria, and how the seismogenic thickness varies across the ocean-continent transition. Finally, we consider the limited seismicity of the off-rift interior of the continent, principally in the Congo basin. In each case, we consider the seismicity, the surface geology, the lithospheric and thermal structure, and the gravity field to provide a coherent picture of the processes controlling the deformation of the region.

2 Data and analysis

2.1 Earthquake seismology

We employ two techniques for the analysis of the source parameters of large African earthquakes. For earthquakes where a clear teleseismic signal is seen at a large number of stations, inversion of the full waveform for both P and SH waves yields estimates of the centroid depth, seismic moment, source time function and focal mechanism. Whilst estimates for these parameters are available through routinely determined catalogues such as the gCMT (Dziewonski et al. 1981; Arvidsson and Ekstrom 1998; www.globalcmt.org) and the EHB (Engdahl et al. 1998 and later updates), body-waveform modelling such as that used here provides a significant increase in the accuracy of the parameters determined. This technique is typically limited to earthquakes of $M_W \geq 5.5$, although it can occasionally be applied to smaller events when the signal is exceptionally clear.

For events where full inversion is not possible, due to limited station coverage or small signal amplitude, but where the initial P arrival and that of subsequent depth phases can be seen at a limited number of stations, we attempt to determine the centroid depth only though forward modelling to match the depth phase delay. This technique was tried for many earthquakes in the study area with magnitudes $M_W \geq 5.0$. However, seismograms with a very low noise content are required for events with lower amplitudes, and only a small number of those attempted yielded reliable results.

We present a total of 55 new solutions determined by full waveform inversion (Table 1), along with a further 57 centroid depths determined through forward modelling of depth phases (Table 2). These combine with an existing data set of 96 waveform solutions and 19 depth-phase results from previous studies, summarised in Tables 1 and 2. These data were selected from published works using similar methods to that of this study. The full data set is detailed in Figure 1. Full solutions for all new events are available in supplementary material, as are a set of figures with earthquakes labelled by date, rather than depth, for easier comparison with Tables 1 & 2.

2.1.1 Body waveform modelling

Teleseismic data were taken from the IRIS DMC, principally utilising GDSN data, but including other networks where possible. Broadband data were deconvolved through a filter to reproduce the response of a long period 15-100s World Wide Standardised Seismographic Network (WWSSN) instrument. This limitation on the included frequency content firstly allows the source of an earthquake of $M_W \approx 6$ to be modelled as a finite-duration rupture at a point source (the centroid), and secondly limits the sensitivity of the resultant waveform to the finer variations in the velocity structure of the source region, allowing a relatively simple velocity model to be used. We then use the MT5 program of Zwick et al. (1994), a version of the algorithm of McCaffrey and Abers (1988) and McCaffrey et al. (1991), to jointly invert both P and SH waves, taken from stations in a epicentral distance range of $30 - 90°(P)$ and $30 - 80°(SH)$. Stations were checked for the clarity of arrivals in both broadband and filtered data, and then weighted according to azimuthal distribution during inversion, with SH seismograms additionally being weighted at 50% of that of P seismograms, to compensate for their increased amplitude. The program is limited to inverting a total of 50 seismograms, and for events where more than this number of clear seismograms are available, stations were selected to retain the best possible azimuthal and epicentral coverage. The program inverts to minimise the misfit via a least-squares routine between the observed seismogram over a window containing the P, pP and sP, or the S and sS phases, and a calculated synthetic seismogram, by varying the focal mechanism, centroid depth, moment, and source time function.

Whilst accurate velocity models (e.g., Prodehl et al. 1997; Mackenzie et al. 2005; Maguire et al. 2006; Cornwell et al. 2010) and density models (e.g., Cornwell et al. 2006), exist for several regions of Africa, the coverage of such studies is spatially very limited, due to the logistical constraints on data acquisition. Due to the wide variety of areas considered in this study, and the lack of detailed information regarding the velocity structure at the location of every earthquake, we assumed a generic model with parameters estimated to be an average across all the regions considered, based on the data available from well-studied areas. We used a simple velocity model, consisting of a halfspace of $V_p = 6.5$ ms^{-1}, $V_s = 3.8$ ms^{-1}and $\rho = 2800$ kg m^{-3}. For events occurring underwater, a water layer was added to the velocity model, with a depth as determined using the best available location (EHB or NEIC) and taken from the SRTM30PLUS model (Becker et al., 2009). A degree of flexibility was allowed in the thickness of this layer during inversion, due to the variation in water depth within the limits of the location error. Small variations in the velocity structure, expected to result from discrepancies between our model, averaged both laterally and vertically through the crust, and the actual velocity profile at the location of each earthquake, have only a minor effect on the source mechanism parameters, but are responsible for much of the uncertainty in depth determination (Taymaz et al., 1990). During inversion, the source was constrained to be entirely double-couple. The source time function was defined by a number of triangular elements, and limited to a length reasonable for the magnitude of the event in question. Starting parameters for the inversion were taken from the gCMT catalogue, and the onset time for each station was manually picked from the broadband data where possible.

This technique has been employed in numerous previous studies, and is sufficiently routine not to require explanation in greater detail here. The validity of the point-source assumption is discussed by Nábělek (1984a). Typical errors in the technique are ±4 km for depth, and ±10° for strike, ±5° for dip, and ±10° for rake (e.g., Molnar and Lyon-Caen 1989).

2.1.2 Forward modelling of depth phases

For events where body-waveform inversion was not possible due to low magnitude or limited station coverage, we determine centroid depths though the forward modelling of the P depth-phase delays. For each event, the broadband data from stations where the arrival of the initial P phase along with at least one of the pP or sP depth phases were visible were selected, within the 30–90° epicentral range usable. For events where identification of depth phases was difficult, we utilise a method similar to that of Yang and Chen (2010), converting to the response of a short-period WWSSN accelerometer, which often improved the signal-to-noise ratio of short duration, small magnitude events. Synthetics were calculated using the WKBJ algorithm (Chapman, 1978; Chapman et al., 1988), based on the location of the station relative to the source, assuming the mechanism from the gCMT catalogue, and then aligned based on the peak of the first arrival. Depth was altered manually to obtain the best fit for the delay time between initial and depth phases for observed and synthetic data. The WKBJ algorithm requires a whole-earth velocity model, and for this we used the `ak135` model (Kennett et al., 1995), again with a water layer added if required based on the best available source location. Errors are typically ± 3 km in depth, except at depths less than $\sim$10 km, when identification of individual phases becomes difficult due to overlap, with increased error bounds as a result.

Attempts were made to fit the relative amplitude of the peaks, but the absolute amplitude of the synthetic was simply scaled to fit that of the observed data. No attempt was made to determine the source time function — a simple pulse source was used in all models — however, given the low magnitude of the events this technique was applied to, this is not problematic. For several events, the polarity of one or more of the synthetic phases is reversed from that of the observed data, although the fit of the relative arrival time is good, indicating that the adopted mechanism is incorrect. Due to a lack of coverage of the focal sphere, we made no attempt to modify the mechanism from the pre-determined gCMT mechanism to compensate for this. Several events were modelled for which no gCMT mechanism was available, or the given mechanism did not match the majority of the waveform data. In these cases, a mechanism based on the local strain field was assumed for the purposes of modelling, and checked for consistency with the observed seismograms.

2.2 Seismicity catalogues

We also use a number of other earthquake catalogues. An updated version of the EHB catalogue (Engdahl et al., 1998) has been used extensively for the geographic location of the earthquakes in this study, and of smaller earthquakes when considering the distribution of seismicity in a geographic context. As an extension to the magnitude range available from the EHB catalogue when considering the seismicity of NW Africa, we also make use of the full ISC catalogue, along with the Centennial Hypocentre catalogue, which provides locations and approximate depths for major earthquakes since 1900 (Engdahl and Villaseñor, 2002). A number of local seismic studies have been used along the EARS, from Afar to Rukwa, and are discussed within the context of the teleseismic results we present, and within our understanding of continental tectonics. Further local studies are considered in NW Africa. Investigations into historical seismicity (e.g., Ambraseys and Adams 1991; Ambraseys et al. 1994) are considered when assessing regional seismogenic potential.

2.3 Lithospheric mapping

The lithosphere is defined as the part of the crust and upper mantle in which heat transport is dominated by conductive rather than convective processes. Numerous methods have been employed in the attempt to determine the lithospheric thickness of continental regions, spanning surface-wave studies, seismic anisotropy, receiver functions, magnetotellurics, electrical resistivity, heat flow models, and mantle nodule thermobarometry. All of these methods have different advantages and draw-backs, but the principle issue is the difficulty in determining the thermal structure of the earth at depth from indirect measurements. As the base of the lithosphere corresponds to a change in the temperature gradient, and not a step change in either temperature or composition, it is not expected to correspond to a seismic discontinuity that can be directly imaged. For a full discussion of these various methods, and the issues involved, see Eaton et al. (2009) and Artemieva (2009).

In this study, we use the lithospheric thickness maps of Priestley and M^{c}Kenzie (2006) and subsequent updates for Africa. The construction of such maps utilises fundamental and higher-mode surface-wave tomography to determine the variation in shear-wave velocity as a function of depth $V_s(z)$, with conversion to temperature structure $T(z)$, using an empirical parameterisation based on observations from the Pacific. The base of the lithosphere is defined by the depth of the rapid change in thermal gradient across the thermal boundary layer, representing the change between a conductive-dominated geothermal gradient to convective-dominated geothermal gradient. It is determined by fitting theoretical geotherms to the depth-dependent temperature structure obtained from the surface-wave tomography on a $2° \times 2°$ grid. Technical limitations in the procedure limit its use to regions where the lithospheric thickness is greater than $\sim$ 110 km. For regions with smaller lithospheric thickness, only an upper limit can be determined. The resolution of the maps produced is $\sim$ 300 km (lateral) and $\sim$ 25 km (vertical), dependent on path coverage. A more detailed description of the mapping techniques, including discussion of the limitations and resolution is given in Priestley and M^{c}Kenzie (2006) and Priestley et al. (2008). The updated version included here for East Africa results from an significant (approximately five-fold) increase in the volume of surface-wave data available for the initial tomographic inversion, and from the use of slightly less restrictive limits on the depth range of temperature data used when fitting theoretical geotherms, checked for reliability against predictions from thermal profiles fixed at greater depths.

The method of Priestley and M^{c}Kenzie (2006) determines lithospheric thickness based on the temperature structure of the upper mantle, and in principle is only directly comparable to measurements of lithospheric thickness derived from fitting theoretical geotherms to mantle nodule thermobarometry data.

2.4 Gravity data

We use long-wavelength free-air gravity anomaly data, taken from Pavlis et al. (2008), computed using spherical harmonic coefficients taken from GRACE gravity data (www-app2.gfz-potsdam.de/pb1/op/grace/results). Data are filtered in the pass range $500 \leq 4000$ km, and used to construct a $1° \times 1°$ grid.

3 Africa-Arabia Extension - Red Sea and Gulf of Aden

3.1 Rifting and extension

As Arabia has moved northwards from Africa, continental extension and rifting has given way to seafloor spreading along the Red Sea and the Gulf of Aden, joining up with the Carlsberg ridge in the Indian ocean to the east, and linking up with the Dead Sea Transform system and the Anatolian faults in the northwest. The two new oceanic basins meet the EARS at the Afar triple junction, a region that is currently in the final stages of evolving from continental to oceanic extension. We consider a total of 49 earthquakes in this region, of which 26 are new to this study (Figure 2).

The general seismicity of oceanic ridges is well understood (e.g., Rundquist and Sobolev 2002), with earthquakes generally limited to depths of ≤10 km below the seabed, in agreement with the depth of the 600°C isotherm (M^{c}Kenzie et al., 2005). Events along the active spreading ridges of Aden and the Red Sea are confined to centroid depths of ≤11 km below sea or land surface (Figure 2). This small seismogenic thickness is consistent with their occurrence in hot, weak, newly formed oceanic lithosphere. The same depth distribution is also seen in Afar (inset, Figure 2), which is in the final stages of continental breakup (e.g., Keir et al. 2009; see section 4.2).

Seismic activity in the Red Sea is dominated by NE-SW extension perpendicular to the spreading axis. Two events (at ∼34°E, 27°N) in the Gulf of Suez, modelled by Huang and Solomon (1987) and by Jackson et al. (1988) may be attributed to the continuation of slow extension at the southern end of the Gulf. Earthquakes in the Gulf of Aqaba display a variation between extension and left-lateral strike-slip, consistent with oblique slip as motion from the Red Sea is transferred to the Dead Sea Transform though a series of left-stepping pull-apart basins (Ben-Avraham, 1985; Baer et al., 2008). In this region, the seismogenic thickness is slightly greater than that seen along the active spreading ridges, with the earthquake of 22 November 1995, M_W 7.1, having a centroid of 15 km. This is consistent with a slightly colder, stronger lithosphere where the component of extension is slow.

In the Afar region seismicity is dominated by shallow extension (Figure 2), with a rotation in extension direction from $\sim$ N-S in the east, to NNE-SSW in the west, consistent with the change in extension direction between the Gulf of Aden and the Red Sea. A review of seismicity in the region from 1960-2000 (Hofstetter and Beyth, 2003) finds similar trends in the small-scale seismotectonics of the Afar triple junction. Seven of the 23 events studied in the Afar region have significant strike-slip motion, most probably linked to offset between rift segments. Seismicity in this region is covered in greater detail within the context of the EARS in section 4.2.

Of the ten events from the past $\sim$30 years in the Gulf of Aden with $M_W \geq 5.5$, nine display right-lateral strike-slip mechanisms on NE-SW planes, concentrated along major transform faults (Figure 2). The two most active groups of these events occur at the eastern end of the Gulf where the ridge enters the Indian ocean, and correlate with the transforms with the greatest ridge offset, concentrated between active ridge segments. This seismic behaviour along the Gulf of Aden contrasts with that along the Red Sea, where the ridge is relatively straight. With no major offsets between Afar and the gulfs of Aqaba and Suez, seismic activity along the Red Sea ridge is dominantly ridge-perpendicular extension.

Total slip along a transform fault between sections of active ridges must occur at a rate equal to that of the full-ridge spreading rates. Spreading along the ridges is dominantly accomplished though magmatic extension, which we expect to have relatively low seismic moment release (e.g., Cowie et al. 1993; Wright et al. 2006). In contrast, motion along the major transforms is amagmatic, and hence, whilst slip may occur aseismically, inter-ridge transform segments have a much greater seismogenic potential per unit length that the ridge itself, which may explain why the majority of the large earthquakes in this extensional region are strike-slip, rather than normal faulting.

3.2 Margins of the Red Sea

On 15 May 2009, a series of earthquakes, two of which are presented here, occurred at 25.20°N 37.76°E in Saudi Arabia, on the Arabian margin of the Red Sea. This region is associated with the Harrat Lunayyir volcanic field, and studies of these earthquakes using satellite interferometry indicate that the earthquake sequence was associated with dyke injection parallel to the margin (Baer and Hamiel, 2010; Pallister et al., 2010). A similar set of events occurring in 2005, near Tabuk, Saudi Arabia (27.8°N, 36.9°E, Figure 2) were studied using regional, rather then teleseismic waveform inversion, and also indicate extension aligned with the NE-SW Red Sea extension, although the possibility of a magmatic component was not investigated (Aldamegh et al., 2009). All of these events show rupture at shallow depths of 3–4 km. Intermittent small scale seismicity is record along the margin, down to Yemen.

It is notable that whilst a number of events have occurred along the Arabian margin, instrumental catalogues do not record any events of significant size along the African margin. Similarly, historical evidence records substantially greater seismic activity along the Arabian margin than along the Africa margin (Amraseys and Melville, 1989; Ambraseys et al., 1994). Whilst the largest instrumentally recorded event on this NE margin of the Red Sea is of $M_W \approx 5.7$, historical evidence records several much larger events, up to an estimated $M_S \approx 7$ event in 1068AD (Ambraseys et al., 1994), which may represent a significant seismic hazard along the Arabian margin of the Red Sea.

Increased seismic activity along the Arabian margin of Red Sea, in contrast to the

Africa side, corresponds to a marked difference in the elevation of the respective margins (Figure 3a). In turn, the elevated topography of the Arabian margin correlates with a large free-air gravity anomaly (Figure 3b), which is not present under the African margin. Studies of this anomaly associate it with a low-velocity region in the upper mantle, likely to be a mantle upwelling, resulting in the observed gravity anomaly, and dynamically elevating the region (Daradich et al., 2003). This region is also the site of increased volcanic activity, corresponding to the regions with positive gravity anomalies (Figure 3b), raising the possibility that the region has been subject to magmatic underplating, further increasing the elevation.

Figure 3c presents topographic and gravity swaths, taken in the areas of the boxes from Figure 3a,b, along with earthquake data projected onto the central line of the swath area. The long-wavelength gravity corresponds with the extent and magnitude of long-wavelength variations in the topography, at an admittance of $\sim$50 mGal/km, indicating convective support of there region. The main peak in seismicity corresponds to the oceanic rift at the centre of the Red Sea (blue box, Figure 3c). A secondary peak in seismic activity occurs, centred slightly seaward of the peak in the topography of the Arabian margin (yellow box, Figure 3c), which is not seen on the African side. This occurs at the edge of the positive gravity anomaly under Arabia. We suggest the the localisation of these earthquakes, and their related magmatism, results from the gravitationally-driven reactivation of relict extensional structures, present at the margins of the original continental rift. The lack of seismic activity further into the Arabian peninsula (Figures 3a,c; Ambraseys et al. 1994), where the gravity anomaly is highest, and where volcanic activity continues, indicates a strong structural control on the occurrence of these earthquakes, modulating the forces induced by the epeirogenic change in gravitational potential.

4 The East African Rift System

4.1 Geodynamics

The East African Rift System (EARS, Figure 4) consists of a series of connected continental rifts separating the main African (Nubian) plate from the Somali plate, and the Indian Ocean. Geodetic observations have been used to suggest the existence of several microplates acting as rigid blocks between discrete sections of the rift system, in Tanzania, and between Madagascar and the East African coast (e.g., Stamps et al. 2008). In Figures 5 and 6, we present 36 new solutions from waveform modelling, along with 50 depths from depth-phase forward modelling. A further 86 events were studied by others, most notably Foster and Jackson (1998) and Yang and Chen (2010).

The rift system can effectively be considered in three parts; Afar and the Main Ethiopian rift in the north, the western branch, and the eastern branch. Within each rift segment, focal mechanisms are dominated by E-W extensional faulting. Extension in other orientations is occasionally seen along some of the minor rifts distributing deformation away from the main rift branches, for example, at the Kariba and Mweru rifts, off the western branch, where normal faulting earthquakes occur with T-axes aligned NW-SE. At all points along the rift system, extensional faulting is dominantly perpendicular to the local rift, with few earthquakes involving a significant oblique slip component.

At major offsets in the rift, such as along the Aswa shear zone, or at Rukwa, transtensional motion is seen (Figures 5,6). The Darfur earthquake sequence of 1990-1991 shows evidence for oblique slip along the reactivated Aswa shear zone, which offsets the western and eastern branches to the south from the Main Ethiopian rift to the north, into a minor extensional component aligned ∼NNW-SSE and a major sinistral strike-slip component. Previous studies note that whilst the mainshock was strike-slip, all of the large aftershocks were extensional (Gaulon et al., 1992). Mechanism orientation for this sequence of earthquakes may either indicate an approximately uniform slip vector on a rupture plane of variable strike, or a change in the orientation of the localised principle stress direction following the mainshock.

South of the Aswa shear, the rift system splits into two. The western branch is seismically active along its entire length, from Uganda to Mozambique, with further distributed deformation to the west of the main rift. The eastern branch is shorter and less well defined in the south, where it becomes progressively more distributed into Tanzania (Figure 4). Seismic activity along this branch of the rift is less common than along the western branch (Foster et al. 1997; Figures 5, 6).

GPS surveys indicate that extension in the EARS is fastest at the northern end of the Main Ethiopian rift, at $\sim$6.5 mm/yr, decreasing southwards to $\sim$1 mm/yr in Mozambique (Stamps et al., 2008). Where the rift separates into western and eastern branches, the geodetic models of Stamps et al. (2008) indicate a southwards decrease in extension rate ($\sim$4 – 0.1 mm/yr) across the eastern branch, matched by a southwards increase in extension rate($\sim$1.5 – 4 mm/yr) across the western branch between the Aswa shear zone and the Rungwe triple junction.

4.2 Seismogenic thickness

A number of previous studies have noted the presence of earthquakes in the lower crust in parts of the EARS (e.g., Chen and Molnar 1983; Shudofsky 1985; Nyblade and Langston 1995; Foster and Jackson 1998; Yang and Chen 2010). The crustal structure of the rift has been investigated in several places, by receiver function studies (e.g., Last et al. 1997; Dugda et al. 2005; Cornwell et al. 2010), refraction studies (e.g., KRISP project, Prodehl et al. 1994, 1997), and travel times for *PmP* phase arrivals (Camelbeeck and Iranga, 1996). Typical values place the Moho at 40-44 km beneath the western branch and 37-42 km beneath the eastern branch. Crustal thicknesses in Afar of 13-28 km are consistent with higher extension factors and thinner crust at the northern end of the Main Ethiopian rift (Dugda et al., 2005). Crustal thickness along the rift is presumed to increase with decreasing extension factor southwards along the Main

Ethiopian rift through Turkana up to the 40 km values seen in places around southern Kenya and Tanzania. Around Rukwa and Lake Tanganyika, both receiver function analysis and PmP phase analysis find crustal thicknesses of 40-44 km (Camelbeeck and Iranga, 1996; Dugda et al., 2005).

The exception to this is around Lake Turkana itself, where the EARS crosses the Mesozoic NW-SE trending Anza rift, which thinned the crust prior to the current extension phase (Hendrie et al., 1994). This is likely also to be linked to the lower topography seen at Turkana compared to regions to the north and south, although there are also epeirogenic effects affecting topography. Off-rift crustal thicknesses are generally 35-45 km, with larger values found across the Ethiopian Plateau related to magmatic underplating of the crust (Keir et al., 2009).

Within the network of Archean cratons and early Proterozoic belts (Figure 9a), crustal thickness does not correlate consistently with either topography (e.g., Figure 5), or with regions of prior and current extension (Figure 9b), but appears to be inherited from the geology of the Precambrian basement in each region. Crust is often thicker in the mobile belts of eastern and southern Africa (e.g., Ubendian, Usagaran, Limpopo belts) than the cratons they surround (Last et al., 1997; Nguuri et al., 2001; Nair et al., 2006).

Figure 8 shows histograms of earthquake centroid depths from this study, split into regional groups outlined in Figure 7. In Afar, centroids are concentrated at <11 km, and are confined to the upper crust only, consistent with constraint by the expected 350° isotherm. We exclude results from Hagos et al. (2006), who inverted P and SH teleseismic waveforms to investigate source parameters for seven events in Afar, and obtained centroids of 17-22km. Five of these events have been modelled independently by others (Foster and Jackson 1998; Ayele et al. 2007, this study), all of whom obtained depths of 11 km or less. We attribute this difference to the bandwidth of the filter applied to the broadband data during seismogram preparation, where Hagos et al. (2006) removed the higher-frequency components, resulting in a much broader signal, matched by a deeper source with an unusually long source time function for events of this size. We therefore consider these depths to be unreliable, although the mechanisms from all studies are similar.

A local seismic study by Keir et al. (2009) in Afar and the Main Ethiopian Rift (Box B, Figure 7) found microearthquakes throughout the upper crust across the region, and extending down to 20-30 km in discrete patches. These are associated with seismically determined concentrations of partial melt, and with locations of prominent clusters of volcanoes, and hence are attributed to fluid migration in magmatic rifts, as seen elsewhere, in New Zealand, Iceland, and Hawaii (Wright and Klein, 2006; Reyners et al., 2007; Keir et al., 2009; Soosalu et al., 2009). These microseismic events are associated with volcanic activity, and are possible in the lower crust because of the high strain rates achieved during fluid migration. They are not relevant to the volcano-free background seismicity that is the focus of this study.

Along the western branch of the rift, larger magnitude earthquakes are recorded throughout the crust, down to depths within error of the Moho ($\sim$44 km beneath southern Malawi, Figure 6). Earthquakes within the lower crust, at depths where the temperature is likely to be $\geq 350°$, occur along the entire length of the western rift from southern Sudan to Mozambique.

The eastern branch presents a more complex picture. It is less seismically active than the western branch, due to a combination of slower extension rates and possibly an increased magmatic contribution to the extension (Calais et al., 2008). Sparse seismicity is recorded extending down to 34 km in isolated patches. However, these can be separated into two laterally distinct patches, one confined to <10 km, the other down to greater depths, as discussed in Section 4.3.

This variation in seismogenic thickness is also seen in a number of local seismic surveys, in the geographic boxes in Figure 7. In box A, central Afar, local and regional seismicity studies determine a seismogenic layer extending down to 14 km (Jacques et al., 1999). The local network study of Lépine and Hirn (1992) finds a similar depth

($\leq$18 km) for the seismic-aseismic transition over a slightly larger area extending out into the Gulf of Tadjurah. Box B represents the study area of Keir et al. (2006, 2009), who found seismicity through the upper crust all along the rift, and discrete patches of volcanism-related lower crustal seismicity. In box C, a microearthquake study by Young et al. (1991) detected seismic activity down to depths of 16 km, with the majority concentrated at $\leq$12 km. Comparing the depth distribution of earthquakes, and crustal heat flow values, to other regions of continental rifts, they suggest that this section of the Kenya rift is typical, with the seismogenic layer confined by the 350°C isotherm.

In box D, microearthquake focal depths are reported down to $\sim$15 km in the northern part of the survey area, and down to $\sim$25 km in the south part of the survey area (Ibs-von Seht et al., 2001). Slightly further south, around Lake Balangida, Nyblade et al. (1996a) operated a local network of seismometers (Box E) with a station spacing of $\geq$50 km, greater than both the deepest seismicity and the thickness of the crust, which severely limits the accuracy of depth determination. Nonetheless, after careful selection of the 23 best located events (Nyblade et al., 1996a; Albaric et al., 2009a), microearthquakes were determined to occur at depths between 10 and 40 km, with errors of $<$ 5 km. The proximity of studies by Ibs-von Seht et al. (2001) and Nyblade et al. (1996a), and the difference in seismogenic thickness seen, indicates a rapid transition in lower crustal rheology going north to south along the Eastern Branch.

On the western branch, studies at the northern end of the Ruwenzori belt (box F) find seismicity down to depths of $\sim$40 km (Tugume and Nyblade, 2009). Around the Rukwa area (box G), a study by Camelbeeck and Iranga (1996) found microearthquakes extending continuously down to 34 km, with a few events at greater depths down to 40 km. These studies agree with the teleseismic earthquake results, which finds earthquakes down to similar depths in both regions, and along much of the western branch.

4.3 Lithospheric thickness

Figure 9c shows earthquake depths together with the lithospheric thickness of East Africa, updated from Priestley et al. (2008). Along the northern sections of the EARS, the lithosphere is too thin (<110 km) to be accurately imaged using the techniques of Priestley and M^{c}Kenzie (2006). We expect the off-rift lithosphere to be of a thickness consistent with the maximum stable thickness of the lithosphere in the oldest oceans, limited by the development of convective instabilities to $\sim$100 km (M^{c}Kenzie et al., 2005).

Notably, nearly all continental earthquakes that occur in the lower crust occur within, or in close proximity to, regions where the lithosphere is resolvably thick (>110 km, Priestley and M^{c}Kenzie 2006 and updates). Additionally, the transition from seismicity being confined to the upper crust along the northern sections of the rift to seismicity extending throughout the crust occurs at the transition to thick lithosphere in all places, within the $\sim$300 km lateral resolution of the techniques applied, as demonstrated by the cross section in Figure 10. Whilst events on the cross section are projected onto the line of section, as can be seen from map view, all continental events with centroids >20 km occur within $\lesssim$100 km of regions with lithosphere thicker than 110 km.

Studies of lithospheric thickness along the Main Ethiopian Rift using receiver functions and surface wave dispersion (e.g., Dugda et al. 2007) attempt to infer the depth of the lithosphere-asthenosphere boundary directly from variations in seismic velocity, despite the base of the lithosphere corresponding to a change in temperature gradient, and not a step change in temperature or composition that could result in a seismic discontinuity. This difference in methodology makes direct comparison to the methods and results of Priestley and M^{c}Kenzie (2006) difficult. These studies typically indicate that, under the very northern most sections of the rift near Afar, where the extension factors are highest, and rifting has progressed furthest, the lithosphere has been thinned appreciably from its pre-rift, steady-state thickness. All regions where such thinning has taken place demonstrate seismogenic thicknesses of 15 – 20 km or less.

The contrast between upper crustal seismicity in regions of thinner lithosphere and whole-crustal seismicity in regions with thicker lithosphere is seen particularly clearly in northern Tanzania. In northern Tanzania, the eastern branch of the EARS splits into three separate segments (Figure 11). The Pangani branch goes southeast and eventually links up with the marginal extensional basins along the Tanzanian coast. The westernmost segment enters the Tanzanian craton (Figure 9a) along Lake Eyasi, and rapidly dies out (Foster et al., 1997). The central Manyara-Balangida branch passes around the edge of the Tanzanian craton, at least on the surface, passing along a system of aseismic extensional depressions, before linking up with the western branch at the Rungwe triple junction, between Rukwa and Lake Malawi (Nilsen et al., 2001).

The Pangani branch is seismically inactive, other than a single event, discussed later. Along the Manyara-Balangida branch, 11 events near Lake Natron have well determined depths, all with centroids at $<$10 km. Moving south to Balangida, eight events with from Brazier et al. (2005), Yang and Chen (2010), and this study, indicate the the seismogenic thickness here extends down to $\geq$34 km. Ebinger et al. (1997) and Foster et al. (1997) attribute the deeper southern earthquakes to the Manyara-Balangida rift entering the Tanzanian craton at depth, although the surface expression of the rift is within the Mozambique belt. In contrast, Albaric et al. (2009b) infer, from local seismicity studies, that rupture at Manyara passes into a set of Proterozoic sutures around the craton edge at depth, and not into the Archean craton itself. On the eastern branch histogram, Figure 8, dark grey is used to indicate these deeper events along the craton boundary.

The sharp transition, over $\sim$100 km, from normal to large seismogenic thicknesses in this region coincides with a transition in lithospheric thickness, given that the horizontal resolution of the seismological mapping technique is $\sim$ 300 km, (Priestley and M^{c}Kenzie, 2006). Lithospheric thickness estimates determined from fitting theoretical geotherms to pressure-temperature estimates from nodule data have been determined for two non-diamondiferous kimberlites across this boundary (Priestley et al., 2008). Values of 88 km at Chyulu and 146 km at Labiat (white diamonds, Figure 11) are in agreement with the seismologically determined location of the gradient in lithospheric thickness. Additionally, Cr/Ca array barometry at the Mwadui kimberlite indicates lithospheric thicknesses in excess of 160 km (Tainton et al., 1999; Grütter et al., 2006) (grey diamond, Figure 11). The location of the gradient in lithospheric thickness is consistent across all techniques, and is in the same position as the transition in seismogenic thickness.

Local studies in this region by Nyblade et al. (1996a) and Ibs-von Seht et al. (2001) (discussed above) show a similar contrast in seismogenic thickness across this lithospheric boundary. A more recent study by Albaric et al. (2009b) studied two earthquake swarms, one at the southern most end of Lake Manyara, and another right at the edge of the deployed network, further north at the southern end of Lake Natron (dashed boxes, Figure 11). At Natron, seismicity was determined to be at depths down to 15 km, where as at Manyara, it extended to ~40 km, again demonstrating the difference in seismogenic character between regions where the lithosphere is thick, and regions where it is thin.

Earthquakes as deep as 26 km are seen in Madagascar, although the region is not determined to be underlain by resolvably thick lithosphere using the method of Priestley and M^{c}Kenzie (2006). However, based on the presence of Archean basement (the Antanarivo craton, Figure 9a), which often correlates with thick lithosphere, and the small area of Madagascar, it is entirely possible that a region of thick lithosphere of insufficient lateral extent to be detected by surface-wave tomography may exist under Madagascar. Madagascar also lies on the edge of the area used in the surface-wave inversions of Priestley and M^{c}Kenzie (2006), Priestley et al. (2008) and the update used here, where the path coverage is poor, leading to a less well constrained velocity model.

4.4 Tectonic structure

Increased seismogenic thickness (Figure 5,6) is also limited to areas with dominant tectonothermal ages of $\geq$1500 Ma (Figure 9a), which also correspond to areas of increased lithospheric thickness (Figure 9c), although neither correlation is as clear as the correspondence between seismogenic and lithospheric thicknesses. Where the rift passes through the Neoproterozoic East African Orogen and other regions formed in the Pan-African Tectonothermal Event (Meert, 2003), seismicity is usually limited to the upper crust. In older regions, it typically extends to the lower crust (shown as dark grey events in Figure 8).

Figure 9a presents basement ages of formation, and of Phanerozoic activity, compiled after an extensive survey of existing literature. It is compiled and drawn in the style employed in Begg et al. (2009), grouping regions based on their age and method of formation, and noting where possible any large scale reworking, reactivation, or later metamorphism. The uncertainties in the composition of such maps are substantial - basement exposure is often minimal, sometimes non-existent, over large areas, allowing different authors to apply their own interpretation based on the available evidence. The structures represented are also highly three-dimensional, and not easily represented in a map view. For example, the extent of the Zambia craton (Za.C., Figure 9a) is typically given as shown here. However, a recent study by De Waele et al. (2008) proposed that the expression of this Archean block on the surface is actually only a small part of an Archean Likasi terrane that has a much larger extent at depth (dashed brown line, Figure 9a). Similarly, the eastwards extent of the Tanzanian craton at depth remains uncertain. Boundaries in Figure 9a attempt to approximate the location of the change in basement type, but are not likely to be accurate to better than $\sim$100 km. Principle references used in this study are detailed in supplementary material.

Archean cratons and thick lithosphere correlate in their broad location across Africa (Priestley et al. 2008 and Figure 9). Surface-wave tomography reveals resolvably thick lithosphere (>110 km) extending continuously under the Congo, Tanzanian, Zambian, Zimbabwe and Kaapvaal cratons, with the cratons themselves being underlain by regions of lithosphere thicker than that under the surrounding Proterozoic mobile belts. In most places the thick lithosphere of Africa appears to extend beyond the craton boundaries, except where prolonged major subduction has taken place dipping beneath the craton boundary, which would likely re-enrich the depleted lithosphere to the point at which it is no longer gravitationally stable at such thicknesses (e.g., northern Congo, southwestern Congo; Porada 1989; Begg et al. 2009).

The map presented in Figure 9c is an update to that of Priestley et al. (2008), based on a substantially expanded surface-wave data set, and the use of lower-temperature, shallower-depth temperature estimates in the conversion to lithospheric thickness. Based on comparison to the basement architecture (Figure 9a), we are now able to resolve the variation in lithospheric thicknesses between the Archean cratons and many of the Proterozoic mobile belts that separate them, such as the Damaran and Kibaran belts. Many of these mobile belts, where they separate cratonic regions on a scale of hundreds, rather than thousands of kilometres, have lithospheric thicknesses too great to be stable without significant depletion ($\gtrsim$100 km), but thinner than seen beneath the cratons.

Once formed, regions of stable thick lithosphere are not usually associated with internal compression and orogenesis, but instead tend to limit compression to regions around their edges (e.g., North America; M^{c}Kenzie and Priestley 2008). However, in several places, Proterozoic mobile belts of Africa, formed by orogenesis, are located within regions of thick lithosphere (e.g., Kibaran belt, Ubendian belt, Figure 9). It is unlikely that these belts were associated with either strong crust or thick lithosphere prior to orogenesis. These features may be relatively shallow only, with shortening related to their formation halting when the strong cratonic regions (and associated thick lithosphere) collide at depth, leaving the mobile belts as shallow structures only. Alternately, thin lithosphere beneath these regions may have been thickened during orogenesis, forming a band of younger thick lithosphere beneath the mobile belt, between the regions of cratonic thick lithosphere. In this case, geochemical and geophysical arguments require the lithosphere of the mobile belt to have been depleted prior to orogenesis (M^cKenzie and Priestley, 2008).

Lithospheric thickness appears to have little direct effect on localising extension, which is predominantly controlled by crustal structure. It has long been accepted that the EARS reactivates numerous structures within the pre-existing basement, relict from previous tectonic events (e.g., Ring 1994; Ebinger et al. 1997; Chorowicz 2005). These structures are concentrated in the Proterozoic mobiles belts, and hence, where the rift reactivates these structures, it goes around the structurally more homogeneous Archean cratons, although it does pass though areas with apparently thick lithosphere (Figure 9). Regions associated with thick lithosphere can therefore exert some control on rifting by influencing the formation of compressionally derived crustal structure, which can then affect the localisation of rifting by reactivation. Nyblade and Brazier (2002) extend the idea of crustal reactivation to suggest that the transmission of extension from eastern to western branches at $\sim$12 Ma, when the eastern branch propagates southwards into north Tanzania, results from the pre-existing structure of the Kibaran belt being weaker, and preferentially reactivated, compared with the structure at the western edge of the Mozambique belt. Given the typically thicker lithosphere under the Kibaran belt relative to the Mozambique belt, this supports the idea that the localisation of rifting is dominated by the structure of the crust, where the majority of the long-term strength of the plate is expected to be located (Jackson et al., 2008), rather than by the structure of the lower lithosphere.

The existence of regions of pre-existing crustal structure associated with the mobile belts in Africa allows rifting, in reactivating these existing structures, to pass though regions of thick lithosphere, and it is here that increased seismogenic thickness is seen. The concentration of rifts around the edges of cratons, but not necessarily of thick lithosphere, can be seen throughout the Phanerozoic rifting of Africa (Figure 9b), most notably where the rift passes throught the Ubendian belt, with lithospheric thicknesses imaged at $\geq$160 km. A similar scenario to that seen in modern East Africa may have occurred between the West African craton and the North American craton, both underlain by thick lithosphere, with north Atlantic rifting passing along the Appalachians that separated the two cratonic regions (M^{c}Kenzie and Priestley, 2008). In Africa, rifting does pass though the proposed Saharan metacraton, and the Ugandan craton, but both of these structures are enigmatic, and their existence as coherent blocks of Archean crust is in dispute. Neither is underlain by thick lithosphere. Theories for their geological evolution range from their construction through the amalgamation of discrete small Archean blocks in a Proterozoic matrix (Bumby and Guiraud, 2005), to the structural reworking of a craton following prolonged and extensive compression and subduction-driven alteration during the closure of major bounding oceans (Black and Liégeois, 1993; Liégeois et al., 2005).

5 Seismicity of continental margins

5.1 East Africa - extension

The East African continental margin is associated with seismicity related to extension along the EARS. The Pangani segment of the eastern branch links the north Tanzanian divergence with a series of extensional basins along the coast of Tanzania (Figure 12a). Focal mechanisms indicate that E-W extension continues southwards along these basins, reactivating the Davie ridge, an intercontinental transform along which Madagascar was displaced southwards during the opening of the Somali basin (Narin et al., 1991). Seismic activity along the margin is sparse, but is notable in extending down to 40 km (Figure 12a). The transition from continent to ocean across the margin is therefore mirrored in a transition in seismogenic behaviour. The oceanic crust along the margin is >140 Ma old (Figure 12c; Muller et al. 2008), and at this age is expected to be seismogenic down to $\sim$55 km, corresponding to the depth of the 600°C isotherm (M^{c}Kenzie et al., 2005). The precise nature of the crust across this margin is unknown, and whether these deeper events are in oceanic, continental, or transitional crust is uncertain.

5.2 Northeast Africa - compression

Two events on the margin of Egypt are of particular note (Figure 12b), at depths >20 km. One, at 31.4°N, 27.65°E and at 29 km depth, is at the break in slope of the continental shelf. The focal mechanism for this event indicates NE-SW compression. Compression along this margin may be related simply to the buoyancy force across the margin, driven by the difference in pressure with depth above the level of isostatic compensation between the continent and the adjacent ocean (See section 6.2). Alternately, given the orientation of the one reliable mechanism, compression may be related to the trench-parallel compression of the oceanic plate as it curves to subduct beneath the Aegean at the convex Hellenic subduction zone. Shaw and Jackson (2010) identified a number of events in the oceanic plate between North Africa and the Hellenic trench with trench-parallel compressional mechanisms (green focal spheres, Figure 12b), and the events along the Egyptian margin may represent a continuation of this trend. The depth of the event at 29 km, is similar to those in the Nubian lithosphere offshore of Crete (Shaw and Jackson, 2010), and is not surprising, given the Jurassic age of the sea floor, and its expected thermal structure (McKenzie et al., 2005).

The second deep event is at 22 km near Cairo, back from the margin at the southernmost tip of the Nile delta (Figure 12b). The mechanism for this event indicates N-S extension, which we suggest may be due to flexure of the plate in response to the loading of the Nile Delta, mainly deposited during the Neogene. In a similar way to the outer rise at subduction zones, the bending of the plate may be accommodated by brittle failure in extensional faults in the upper part of the plate. An alternate possibility is that this earthquake relates to the distal effects of extension in the Gulf of Suez, to the east.

5.3 Northwest Africa - compression

The Moroccan/Algerian margin of NW Africa is undergoing active compression along the Rif/Tell ranges, related to the collision between Europe and Africa. Figure 13a shows a total of 17 earthquakes in this region. The 10 along the Mediterranean coast are all $\leq$8 km depth, dominated by NW-SE compressional mechanisms. One earthquake of a sufficient size to be modelled with the techniques used here occurred in the Atlas ranges, with a slightly deeper centroid of 19 km. This earthquake coincides with the northern extent of the thick lithosphere in West Africa (Figure 13b) — however, a single event is insufficient to draw any conclusions regarding crustal rheology. A number of deeper earthquakes are reported west of Gibralter within the oceanic plate along the Azores boundary, down to 38 km (Grimison and Chen, 1988b), within the expected seismogenic thickness expected from the age of the oceanic plate.

A number of previous studies have reported deep earthquakes in this region, based on local and regional studies (e.g., Hatzfeld and Frogneux 1981). Figure 13c shows the full ISC, EHB and Centennial Hypocentre catalogues for this region. Figure 13d then shows the same data set, limited to those events listed as having well constrained depths greater than 40 km, although even these are rarely constrained by any depth phase data. The majority of these events are concentrated around the Gibralter area, mostly at <100 km, with a sequence of events at $\sim$630 km beneath Granada (red points, Figure 13D). The box in the same panel outlines the area within which the microearthquake study of Hatzfeld and Frogneux (1981) found earthquakes down to $\sim$150 km. Of the six remaining events beneath NE Algeria and NW Libya few, if any, depth phases are available for accurate determination of the depth.

We suggest that the deeper earthquakes in the western Mediterranean, clearly occurring well below the continental crust, are not associated with continental rheology and tectonics, but are continuing seismicity related to the subduction of Tethyan oceanic lithosphere between the Rif/Tell and the Atlas mountains, and between the Betics of southern Spain and Europe, which effectively halted with the back-arc collision of the

Rif/Tell/Betics on to the continental margins in the early to middle Miocene (Lonergan and White, 1997; Booth-Rea et al., 2007). This being the case, we find no convincing evidence for earthquakes within the mantle of continental origin under northwest Africa. Intermittent seismicity down to >600 km must be related to oceanic slab descent from a now-extinct subduction zone along the Rif-Tell/Africa margin, which remains seismogenic at depth until heating up to $> 600°$C (Wortel, 1986; Emmerson and M^{c}Kenzie, 2007). The relationship between the end of the slab and its junction to the base of the continental crust along the suture of the earlier oceanic basin remains undetermined.

6 Congo basin - compression

6.1 Seismicity and Gravity

The Congo basin (Figure 14) is a complex sedimentary basin within the interior of the Congo craton, where a probable early Phanerozoic/late Precambrian failed rift (Daly et al., 1992) coincides with a large negative free-air gravity anomaly (Hartley and Allen, 1996). The sedimentary fill is, in places, >8 km thick, and dates back to latest Neoproterozoic (Daly et al., 1992; Laske and Masters, 1997).

Whilst the majority of the interior of Africa, away from the rift system, is seismically relatively inactive, six moderate-sized earthquakes have occurred in the Congo basin. We present solutions for four of these, combined with two from Foster and Jackson (1998). Five of these events are compressional, with P-axes approximately E-W. All of these events are shallow (<10 km), with depths consistent with rupture in the top basement, below the sedimentary fill of the basin.

We now investigate possible dynamic influences on the compressional setting of the Congo basin.

6.2 Peripheral plate forces

Several of these events were studied in detail by Ayele (2002), obtaining similar modelling results to this study, who conclude that they result from the far-field effects of ridge push around the boundaries of the African plate, based on the alignment of the principle stress axis with the extension directions of the Mid-Atlantic ridge, the Carlsberg ridge, and the EARS.

The African continent is bordered to the west, south, east, and northeast by active spreading ridges. Peripheral ridge push forces acting on the plate might be expected to result in the interior of the continent being in widespread compression (e.g., Richardson 1992). However, our survey of large magnitude earthquake mechanisms does not find any evidence for compressional faulting resulting from this anywhere in Africa, except the Congo. Indeed, as seen in Figure 1, the interior of Africa is remarkably aseismic. Additionally, a simple model for the lateral pressure difference across the continental margin demonstrates that the expected magnitude of ridge push on the plate margin is approximately matched by an outwards buoyancy force.

Based on assumed isostatic compensation between oceanic and continental columns at the base of 40 km thick continental crust, we expect a force of $\sim 3.1 - 3.2 \times 10^{12}$ N m^{-1} to act outwards across the margin. Estimates for the magnitude of ridge push vary between $\sim 3 \times 10^{12}$ N m^{-1} and $\sim 3.4 \times 10^{12}$ N m^{-1} (e.g., Parsons and Richter 1980; Copley et al. 2010). We hence expect the two forces to cancel out to the extent where the remaining force is unlikely to be of sufficient magnitude to result in deformation of the continental interior.

An exception to this is in cases where the margin is not paralleled by an active spreading ridge — where this is the case, we expect the buoyancy force across the margin to exceed the ridge push, with the resultant possibility of compression across the continent/ocean transition — potentially as seen on the Egyptian margin (Figure 12b).

6.3 Buoyancy forces within a compensated continent

The Congo basin has a low elevation relative to the surrounding areas of the continental interior, in particular the East African plateau to the east and the highlands of southern Africa to the south (Figure 15a). If the continent were in isostatic equilibrium, with no dynamic support of the topography by sub-lithospheric convection, the contrast in topography between eastern and southern Africa and the Congo would result in a compressional force on the Congo.

Based on averages across the continent, we take a reference column of 40 km thick crust at 900 m elevation, and calculate compensated profiles for the Congo basin (elevation ~400 m) and East Africa (elevation ~ 1400 m). The buoyancy force between these two regions is then given by the integral of the pressure difference (ΔP) between the two profiles down to the compensation depth:

$$F = \int \Delta P dz \tag{1}$$

$$= \frac{g\rho_c}{2}({t_1}^2 - {t_2}^2)\left(1 - \frac{\rho_c}{\rho_m}\right) \tag{2}$$

where t_1 and t_2 are the crustal thicknesses of the two columns, and taking densities of $\rho_c = 2800$ kg m^{-3} and $\rho_m = 3300$ kg m^{-3}. Between East Africa and the Congo, this force is calculated to be $\sim 1.1 \times 10^{12}$ N m^{-1}. The horizontal stress is then dependent on the elastic thickness of the plate, which is not well known. Taking reasonable expected end-member values of 20 – 40 km, based on seismogenic thicknesses across Africa, and the observation that elastic thickness is everywhere less than seismogenic thickness (Maggi et al., 2000), we determine the horizontal stress to be ~ 55 – 27.5 MPa.

Given that the region considered encompasses both the compressional setting in the Congo, and the extensional EARS, both of which contain active faults, the force driving the deformation must be sufficient to cause brittle failure in both systems. The horizontal stress must also be resolved onto the shear stress on a given active fault system, typically dipping at between 30 – 60° (Jackson and White, 1989). If we require the shear stress on a fault to be $\geq$10 MPa for rupture to occur (Scholz, 2002), then the forces in a compensated continent are only sufficient if the elastic thickness is at the lower end of what is probable.

However, available data on the crustal thickness of Africa indicate no large-scale correlation between elevation (Figure 15a) and crustal thickness (Figure 15b), indicating that the continent is not in a state where elevation is purely isostatically compensated, a concept reinforced by studies of the gravity field and surrounding ocean bathymetry (Nyblade and Robinson, 1994; Al-Hajri et al., 2009). This being the case, calculations for the buoyancy forces resulting simply from compensated topography are not appropriate for this part of Africa, and are likely to be insufficient to explain the deformation seen.

6.4 Forces resulting from dynamically supported topography

Investigations into the origin of the basement of the Congo using evidence from lithospheric thickness, mantle shear-wave velocity and mantle flow models, gravity analysis and modelling, and subsidence analysis conclude that there is likely to be a modern mantle downwelling coinciding with the pre-existing basin, resulting in the negative free-air gravity anomaly (Figure 14c) and an epeirogenic drawdown of $\sim$400 m air-equivalent loading (Crosby et al., 2010).

The correlation of the few thrust-faulting earthquakes and the relatively low topography of the Congo basin, induced by the dynamic effects of the convective downwelling beneath the region suggests that the location of these earthquakes within Africa may be controlled by the effect of dynamically induced changes in the stress field of the plate.

Anomalies in the long-wavelength free-air gravity field over Africa (Figure 15c) suggest a widespread control from upper mantle convection on the topography of the continent. In the Congo, the negative dynamic topographic effect decreases the elevation. Conversely, across the adjacent East African plateau, the dynamically supported increase in elevation associated with the Afar and Victoria plumes, and the African Superswell (Nyblade and Langston, 1995; Weeraratne et al., 2003), all indicated by positive gravity anomalies, takes the plate out of compression, and into gravitationally driven extension, allowing rifting to take place.

We convert free-air gravity anomalies to an estimated topographic effect resulting from dynamic forces on the base of the plate using a 50 mGal/km conversion, assuming a mantle density of 3300 kg m^{-3} (Figure 15d). This conversion estimates the magnitude of the uplift of East Africa to be ∼500 m, and of the draw-down under the Congo to be ∼-500 m. We model the uplift as a simple vertical shift of the whole mechanical lithosphere, and calculate the force required to maintain the difference in elevation of the plate. For these calculations, we assume a uniform crustal thickness, t_c, of 40 km (based on Bassin et al. 2000), a uniform thickness of the mechanical boundary layer, t_m, of 160 km (based on a value slightly less than the whole-lithosphere thickness of Priestley and M^{c}Kenzie 2006), and densities of $\rho_c = 2800$ kg m^{-3} and $\rho_m = 3300$ kg m^{-3}. The total dynamic force is then given by

$$F = g(\rho_c t_c + \rho_m(t_m - t_c))\epsilon \tag{3}$$

where ϵ is the difference in dynamically induced elevation between two points. The resultant force from across East Africa/Congo is $\sim 5.0 \times 10^{12}$ N m^{-1}. Resolved over the elastic thickness, which we take to be a maximum of 40 km, this gives a minimum plate-parallel stress of 125 MPa. These calculations neglect viscous forces on the base of the plate from the convecting asthenosphere, which we expect to add to the total resultant force between the East Africa and the Congo, further increasing the resolved stresses (e.g., Westaway 1993). The lower limit on horizontal stresses obtained indicates that the effects of dynamically driven topographic contrasts are more than sufficient to account for the deformation seen across equatorial Africa, even taking into account that this includes two deforming regions, the Congo and the East African rift.

We have used a simple two dimensional model to determine dynamically driven stresses, however, the topographic features under consideration are not linear features. If we consider the downwelling under the Congo to be approximately axisymmetric, the forces resulting from the topographic low (but not including the effects of the upwelling under East Africa) must produce a similar axisymmetric pattern of compressional stress, centred on the Congo. The dominant orientation of the deformation is hence expected to be controlled by the direction of maximum force external to the downwelling system, in this case directed from East Africa, approximately E/W. This orientation is in agreement with the orientation of the earthquake focal mechanisms seen (Figure 14a).

7 Discussion

7.1 Rheological implications of seismogenic and lithospheric thickness

Increased seismogenic thickness in Africa is observed to correspond to regions underlain by thick lithosphere (Figures 9,10,11). This fits with a global perspective, where regions with thin lithosphere (e.g., Greece, western USA, western Turkey) have small seismogenic thicknesses, and regions with thicker lithosphere (e.g., East Africa, northern Baikal) have larger seismogenic thicknesses. The presence of a thick conductive lithosphere will provide a degree of thermal insulation for the crust from the convective mantle, depressing the geotherm and increasing the depth of the 350°C isotherm believed to control the seismic-aseismic transition in normal continental crust (Chen and Molnar, 1983). However, the magnitude of this insulation is insufficient to explain the observed seismogenic thicknesses of ≥40 km (M^{c}Kenzie et al., 2005). Additionally, the observed rapid variation in seismogenic thickness is inconsistent with a smooth variation in the seismic-aseismic transition linked directly to the variation in lithospheric thickness. An anhydrous lower crust of granulite-facies material, potentially produced during orogenesis (M^{c}Kenzie and Priestley, 2008), is believed to be sufficiently strong to remain seismic at temperatures well above the 350°C limit. This provides a possible explanation for the observed seismicity (Jackson et al., 2004; Lund et al., 2004). However, such material is metastable at these pressures and temperatures, and the addition of small amounts of fluid can promote the rapid conversion to eclogite (Yardley, 2009), which is much weaker, and would deform through stable sliding and aseismic creep, rather than seismic failure.

One possible factor contibuting to the preservation of a metastable, anhydrous lower crust is the potential for its protection from fluid addition to be aided by an underlying thick lithospheric root. This may provide geochemical insulation for the lower crust, helping to enhance its protection from percolating metasomatic fluids. These fluids, produced at extremely small melt-fractions from within the sub-lithospheric mantle, have volatile-rich compositions which would allow the metastable lower crust to rehydrate (M^{c}Kenzie, 1989; Yardley, 2009). Rising metasomatic fluids may freeze out at depth within the mechanical lithosphere where their solidus temperature exceeds the local geotherm. In regions of thinner lithosphere, where the geothermal gradient is higher, a greater proportion of the metasomatic fluid might penetrate to crustal levels, causing a transformation to a hydrated, weaker mineral assemblage and resulting in a more typical seismogenic profile, confined to the upper crust. The presence of trapped metasomatic layers within the regions of thick lithosphere in East Africa is corroborated by the geochemistry of initial eruptive lavas in the region, which are likely to be sourced from these more-fusable layers within the lithosphere (Furman, 1995, 2007). This hypothesis does not preclude the retention of an anhydrous lower crust in regions with thin lithosphere, and the resultant potential for seismicity down to ∼600°C in such regions, but suggests that the penetration of fluids capable of altering the lower crust is inhibited by a thicker lithospheric root.

Another factor in determining the presence of a strong lower crust is the age of crustal formation or alteration. Large seismogenic thicknesses often correspond to continental regions with basement ages of $\geq$1500 Ma (Figure 9), and two effects contribute to this. Firstly, the depletion of the lithosphere necessary for the stabilisation of a thick lithospheric root, which must occur at shallow depths prior to its thickening, requires levels of melt extraction only likely to have occurred in the Archean (McKenzie and Priestley, 2008). Secondly, the generation of granulite-facies material in the mid to lower crust requires high-temperature conditions within the orogen (England and Thompson, 1984; Le Pichon et al., 1997). Orogenic events that are older, and hence have higher radioactive crustal heat production, will reach granulite facies conditions at smaller orogenic thicknesses than younger events. The amount of orogenic shortening and thickening required to form crustal granulites hence increases through time, making formation less extensive. Older mobile belts required relatively less orogenic thickening to reach the conditions required for the formation of a strong, anhydrous lower crust.

7.2 Seismogenic thickness and fault scaling

The seismogenic thickness, and related crustal strength, of a region has important implications for its geological structure and evolution. Sections of the East African rift with large seismogenic thicknesses often show exceptionally long fault segment lengths, and wide basins (e.g., Ebinger et al. 1999). Jackson and Blenkinsop (1997) studied the Bilila-Mtakataka fault (Figure 16), at the southern end of the Malawi rift, and determined that the fault ruptured in the past in a single large-magnitude event, along a continuous fault scarp over 100 km long, and a single-event offset of $\sim$15 m, in an area where earthquakes have been recorded down to 32 km. At the northern end of Lake Malawi, the Livingston fault shows a fault length of $\sim$100 km, while the width of the half-graben resulting from this major border fault is $\sim$60 km. In Rukwa, Vittori et al. (1997) investigate a number of large (>100 km) faults as candidates for the 1910, M_W 7.4 Rukwa earthquake - the largest recorded earthquake in Africa. Similar large border faults, and wide half-graben basins are seen along Tanganyika, and north to Lake Albert (Rosendahl et al., 1992), all in regions with large seismogenic thickness.

In contrast, other regions of active continental rifting, such as Greece, where the seismogenic thickness is ∼15 km, show fault segment lengths typically up to 20 km (Jackson and White, 1989). The global study of Jackson and White (1989) concluded that fault segment length, down-dip width, and seismogenic thickness all scale with each other. Along with an increasing width of the flexural half-graben resulting from these large border faults, these observations are all indicative of an increased strength of the crust at depth (Jackson and White, 1989; Scholz and Contreras, 1998), which we infer is related to the preservation of metastable anhydrous granulite in the lower crust of the older Proterozoic mobile belts of Africa.

A consequence of the increased dimensions of the fault surface in such regions is that much larger magnitude earthquakes may be possible along the EARS than in typical continental areas. An earthquake occurring on a fault 100 km long, dipping at 45° to 40 km depth, with 10 m slip, as reported by Jackson and Blenkinsop (1997) in Malawi, would have a magnitude of M_W 8.1, and represent a major seismic hazard. Based on the geodetic extension rates in East Africa (Stamps et al., 2008), events on this scale would have recurrence times of at least ∼2000 yrs on each fault, even if a single fault takes up all the extension in that section of the rift. Structure revealed from seismic profiling of the rift basins (Rosendahl et al., 1992) and studies of seismicity in the hanging wall of these large border faults (Biggs et al., 2010) indicates that significant extension is taken up elsewhere across the rift, further increasing the recurrence time of any such earthquakes on the border faults.

7.3 Seismicity at the continent/ocean transition

Seismic activity at the continental margins of Africa displays a combination of the seismogenic behaviours of both continental and oceanic settings. Seismicity of the eastern and northeastern margins extends below the depth limit expected for a purely continental rheology, but not beyond that expected based on the age and thermal structure of the adjacent old oceanic floor. The structure of continental margins is expected to reflect a compositional transition from continental to oceanic cases, following thinning and intrusion of the continental crust during rifting, occurring over a region where the crustal thickness changes from the continental crustal thickness ($\sim$40 km) to the oceanic crustal thickness ($\sim$8 km). After sea floor spreading initiates, and the margin subsequently cools, the entire thinned crust and uppermost mantle may become seismogenic provided the temperature is $< 600^{\circ}$C.

Whilst the majority of non-convergent continental margins are aseismic, the example of Africa shows that seismicity may be induced by a range of possible geodynamic factors. Rapid loading at the continental shelf, associated with the location of major depo-centres, such as the Nile delta, may result in flexural deformation of the margin and brittle failure. Proximity to other regions of tectonic activity may also trigger reactivation of marginal structures, as seen in the case of the East African marginal basins, linked to the proximity of EARS, and in the northeast African marginal compression, potentially linked to the far-field effects of Hellenic subduction. Earthquakes suggest that the young NE margin of the Red Sea displays continuing gravitational collapse of the marginal structures, despite extension having progressed to oceanic spreading at the centre of the rift.

7.4 Affects of mantle convection on continental deformation

Along the margins of the Red Sea, increased seismic and magmatic activity on the Arabian side relative to the African side corresponds to areas of increased elevation and positive gravity anomalies at long wavelengths (500–1000 km), associated with upwelling in the underlying mantle (e.g., Daradich et al. 2003). Seismicity appears to be induced by the increased dynamic elevation of the region, and to be localised within the elevated area by the presence of pre-existing structure along the original continental margin at the edge of the Red Sea.

Peripherial ridge-push on the margins of Africa from the Mid-Atlantic ridge, the Carlsberg ridge, and the ridges in the Red Sea and the Gulf of Aden, mean that the interior of the continent should be in widespread compression (Richardson, 1992). However, the majority of the continent is seismically inactive, implying that the resultant marginal forces are of insufficient magnitude to result in deformation of the continental interior. The exceptions to this occur along the EARS and in the Congo basin. We attribute this broad seismic inactivity to the approximate countering of the ridge-push force on the continental interior by the buoyancy force across the continental margin, to the point where the resultant force is insufficient to result in deformation.

The Congo basin contains the only compressional earthquakes within the continental interior of Africa. The East African rift, and its associated subsidiary rifts, are undergoing active extension. Both of these regions coincide with large scale free-air gravity anomalies. The Congo basin, underlain by a large negative gravity anomaly due to a underlying mantle downwelling, is topographically lowered (Crosby et al., 2010). Along the EARS, widespread mantle upwelling, considered elsewhere in detail (e.g., Ebinger and Sleep 1998; Nyblade et al. 2000) results in positive gravity anomalies, and the epeirogenic uplift of large regions of southern and eastern Africa. Calculations for the forces resulting from the dynamically driven variation in elevation of the mechanical lithosphere indicate that the stress resulting from this effect is sufficient to explain the observed deformation. If the topographic contrasts seen were the result of isostatic compensation of the crust, rather than epeirogenic uplift of the mechanical lithosphere, the resultant stresses for a given elastic thickness are smaller by a factor of $\sim$5. This has implications for the control of mantle convection on the occurrence and localisation of deformation within the interior of a continent, and the associated seismic hazards.

Previous studies have considered the spatial variation in gravitational potential energy (GPE) and vertically averaged deviatoric stresses by considering the lithosphere as an incompressible viscous continuum, and applying the thin-sheet approximation (Ghosh et al., 2009; Stamps et al., 2010). These studies require the continent to be compensated at a pre-determined depth within the mantle, which is achieved by varying the density of the subcrustal layer, rather than modelling the dynamic effects directly.

Delvaux and Barth (2010) invert focal mechanism data from the gCMT catalogue and published literature sources, many of which are included in this study, to determine the present day stress field across Africa, under the assumption that available data is representative of the full seismic cycle. This method also resolves a region of compression in the Congo basin, which they note as coincident with an area of low topography, and attribute the subsequent deformation to low GPE. The broad picture of variation in the stress field from these different assumptions is the same, with topographic elevation dominating over other intra-lithospheric parameters, although the magnitude of the resultant stresses is lower.

Our simple calculations give a force resulting from a 1 km contrast in epeirogenic uplift of $\sim 5.0 \times 10^{12}$ N m^{-1}. In terms of forces determined to be acting on plates, such values are significant. Similar force magnitudes ($5 - 6 \times 10^{12}$ N m^{-1}) have been estimated for the buoyancy force from the Tibetan plateau on India, whilst more minor mountain ranges result in smaller forces (Copley et al., 2010). Estimates for slab pull indicate horizontal tensions in the overlying oceanic lithosphere of $\sim 3 \times 10^{12}$ N m^{-1} (Bird et al., 2008), similar to the approximate magnitude of ridge-push forces ($3.0 - 3.4 \times 10^{12}$ N m^{-1}, e.g., Parsons and Richter 1980). The magnitude of the force in Africa results from the juxtaposition of both upwelling and downwelling convective cells in close proximity, however, the forces resulting from epeirogenic effects elsewhere are still likely be sufficient to influence deformation.

8 Conclusions

Lower crustal earthquakes along the East Africa rift system correlate well with areas of thicker lithosphere, as determined from surface-wave tomography and temperature conversion, and from kimberlite nodule data. A strong, seismogenic lower crust requires a rheology equivalent to that of anhydrous granulite-facies material. Such material is metastable under typical lower crustal conditions, rapidly undergoing conversion to weaker eclogite upon the addition of small amounts of water. We suggest the link between lower crustal seismicity and thick lithosphere may potentially be related to the geochemical insulation of the lower crust provided by the lithospheric root, protecting it from rehydration by percolating metasomatic fluids, sourced from the asthenospheric upper mantle. The strength of this seismogenic lower crust has implications for earthquake hazard in the region, as well as being linked to the size and distribution of major tectonic features in the rift.

Along the continental margins of Africa, we find a low level seismicity induced by a range of geodynamic factors linked to the deformation of regions around the margin. Seismogenic behaviour is consistent with the transition from continental to oceanic rheological models. Nowhere do we find evidence for seismicity in the continental or oceanic mantle at temperatures above 600°C.

We demonstrate the effect of epeirogenic uplift and subsidence on influencing the style and localisation of deformation in the continental interior. Extensional earthquakes along the Arabian margin of the Red Sea indicate the reactivation of relict marginal structures, driven by the increased dynamic elevation of the margin. Compressional earthquakes in the Congo can be produced by the juxtaposition of the East African plateau, elevated by underlying mantle plumes, and the Congo basin, drawn down by a mantle downwelling. Stresses induced by this effect are more than sufficient to result in brittle failure of the plate.

9 Acknowledgements

TJC was supported by a Girdler Scholarship from the University of Cambridge. TJC and JAJ are members of the COMET+ group, within NERC's NCEO. We thank R. Engdahl for providing an updated version of the EHB catalogue. We thank two anonymous reviewers for useful comments that improved this manuscript. Seismogram data was made available though the IRIS Data Management Centre. Landsat imagery was

available through the Global Land Cover Facility (www.landcover.org). ASTER DEM is a product of METI and NASA. A number of figures were made using GMT (Wessel and Smith, 1998).

References

Y. Al-Hajri, N. White, and S. Fishwick. Scales of transient convective support beneath Africa. *Geology*, 37:883–886, 2009. doi: 10.1130/G25703A.1.

J. Albaric, J. Deverchere, C. Petit, J. Perrot, and B. Le Gall. Crustal rheology and depth distribution of earthquakes: Insights from the central and southern East African Rift System. *Tectonophysics*, 468:28–41, 2009a. doi: 10.1016/j.tecto.2008.05.021.

J. Albaric, J. Perrot, J. Déverchère, A. Deschamps, D. Le Gall, R. W. Ferdinand, C. Petit, C. Tiberi, C. Sue, and M. Songo. Contrasted seismogenic and rheological behavious from shallow and deep earthquake sequences in the North Tanzanian Divergence, East Africa. *Journal of African Earth Sciences*, 2009b. doi: 10.1016/j.jafrearsci.2009.09.005.

K. S. Aldamegh, K. M. Abou Elenean, H. M. Hussein, and A. J. Rodgers. Source mechanism of the June 2004 Tabuk earthquake sequence, Eastern Red Sea margin, Kingdom of Saudi Arabia. *Journal of Seismology*, 13:561–576, 2009. doi: 10.1007/s10950-008-9148-5.

N. N. Ambraseys and R. D. Adams. Reappraisal of Major African Earthquakes, south of 20°N, 1900-1930. *Natural Hazards*, 4:389–419, 1991. doi: 10.1007/BF00126646.

N. N. Ambraseys, C. P. Melville, and R. D. Adams. *The Seismicity of Egypt, Arabia and the Red Sea*. Cambridge University Press, 1994.

N. N. Amraseys and C. P. Melville. Evidence for intraplate earthquakes in northwest Arabia. *Bulletin of the Seismological Society of America*, 79:1279–1281, 1989.

I. M. Artemieva. The continental lithosphere: Reconciling thermal, seismic, and petrologic data. *Lithos*, 109:23–46, 2009. doi: 10.1016/j.lithos.2008.09.015.

R. Arvidsson and G. Ekstrom. Global CMT analysis of moderate earthquakes, $M_W \geq 4.5$, using intermediate period surface waves. *Bull. Seis. Soc. Am.*, 88:1003–1013, 1998.

A. Ayele. Active compressional tectonics in central Africa and implications for plate tectonic models: evidence from fault mechanism studies of the 1998 earthquakes in the Congo Basin. *Journal of African Earth Sciences*, 35:45–50, 2002. doi: 10.1016/S0899-5362(02)00098-2.

A. Ayele, G. Stuart, I. Bastow, and D. Keir. The August 2002 earthquake sequence in north Afar: Insights into the neotectonics of the Danakil microplate. *Journal of African Earth Sciences*, 48:70–79, 2007. doi: 10.1016/j.jafrearsci.2006.06.011.

G. Baer and Y. Hamiel. Form and growth of an embryonic continental rift: InSAR observations and modelling of the 2009 western Arabia rifting episode. *Geophysical Journal International*, 182:155–167, 2010. doi: 10.1111/j.1365-246X.2010.04627.x.

G. Baer, G. J. Funning, G. Shamir, and T. J. Wright. The 1995 November 22, M_W 7.2 Gulf of Elat earthquake cycle revisited. *Geophysical Journal International*, 175: 1040–1054, 2008. doi: 10.1111/j.1365-246X.2008.03901.x.

C. Bassin, G. Laske, and G. Masters. The Current Resolution for Surface Wave Tomography in North America. *EOS Transactions, AGU*, 81, 2000.

J. J. Becker, D. T. Sandwell, W. H. F. Smith, J. Braud, B. Binder, J. Depner, D. Fabre, J. Factor, S. Ingalls, S-H. Kim, R. Ladner, K. Marks, S. Nelson, A. Pharaoh, G. Sharman, R. Trimmer, J. VonRosenburg, G. Wallace, and P. Weatherall. Global Bathymetry and Elevation Data at 30 Arc Seconds Resolution: SRTM30PLUS. *Marine Geodesy*, 32:4:355–371, 2009.

G. C. Begg, W. L. Griffen, L. M. Natapov, S. Y. O'Reilly, S. P. Grand, C. J. O'Neill, J. M. A. Hronsky, Y. P. Djomani, C. J. Swain, T. Deen, and P. Bowden. The lithospheric architecture of Africa: Seismic tomography, mantle petrology and tectonic evolution. *Geosphere*, 5:23–50, 2009. doi: 10.1130/GES00179.1.

Z. Ben-Avraham. Structural framework of the Gulf of Eilat (Aqaba), Northern Red Sea. *Journal of Geophysical Research*, 90:703–726, 1985.

M. Bezzeghoud and E. Buforn. Source Parameteres of the 1992 Melilla (Spain, $M_W =$ 4.8), 1994 Alhoceima (Morocco, $M_W = 5.8$) and 1994 Mascara (Algeria, $M_W = 5.7$) Earthquakes and Seismotectonic Implications. *Bulletin of the Seismological Society of America*, 89:359–372, 1999.

J. Biggs, E. Bergman, B. Emmerson, G. J. Funning, J. Jackson, B. Parsons, and T. J. Wright. Fault identification for buried strike-slip earthquakes using InSAR: The 1994 and 2004 Al Hoceima, Morocco earthquakes. *Geophysical Journal International*, 166: 1347–1362, 2006.

J. Biggs, E. Nissen, T. Craig, J. Jackson, and D. P. Robinson. Breaking up the hanging wall of a rift-border fault: The 2009 Karonga earthquakes, Malawi. *Geophysical Research Letters*, 37, 2010. doi: 10.1029/2010GL043179.

P. Bird, Z Liu, and W. K. Rucker. Stresses that drive the plates from below: Definitions, computational path, model optimization and error analysis. *Journal of Geophysical Research*, 113, 2008. doi: 10.1029/2007JB005460.

R. Black and J-P. Liégeois. Cratons, mobile belts, alkaline rocks and continental lithospheric mantle: the Pan-African testimony. *Journal of the Geological Society of London*, 150:89–98, 1993.

G. Booth-Rea, C. R. Ranero, J. M. Martínez-Martínez, and I. Grevemeyer. Crustal types and Tertiary tectonic evolution of the Alborán sea, western Mediterranean. *Geochemistry, Geophysics, Geosystems*, 8(10), 2007. doi: 10.1029/2007GC001639.

J. Braunmiller and J. Nábêlek. The 1989 Ethiopia earthquake sequence. *EOS, Transactions, American Geophysical Union*, 76, 1990.

R. A. Brazier, A. A. Nyblade, and J. Florentin. Focal mechanisms and the stress regime in NE and SW Tanzania, East Africa. *Geophysical Research Letters*, 32, 2005. doi: 10.1029/2005GL023156.

A. J. Bumby and R. Guiraud. The geodynamic setting of the Phanerozoic basins of Africa. *Journal of African Earth Sciences*, 43:1–12, 2005. doi: 10.1016/j.jafrearsci.2005.07.016.

E. Calais, N. d'Oreye, J. Albaric, A. Deschamps, D. Delvaux, J. Déverchère, C. Ebinger, R. W. Ferdinand, F. Kervyn, A. S. Macheyeki, A. Oyen, J. Perrot, E. Saria, B. Smets, D. S. Stamps, and C. Wauthier. Strain accommodation by slow slip and dyking in a youthful continental rift, East Africa. *Nature*, 456, 2008. doi: 10.1038/nature07478.

T. Camelbeeck and M. D. Iranga. Deep crustal earthquakes and active faults along the Rukwa trough, eastern Africa. *Geophysical Journal International*, 124:612–630, 1996.

C. Chapman. A new method for computing synthetic seismograms. *Geophysical Journal of the Royal Astronomical Society*, 45:481–518, 1978.

C. Chapman, C. Yen-Li, and D. Lyness. The WKBJ seismogram algorithm. In D. Doornbos, editor, *Seismological algorithms: Computational methods and computer programs*, pages I.2,47–74. Academic Press Limited, London, 1988.

W.-P. Chen and P. Molnar. Focal depths of intracontinental and intraplate earthquakes and their implications for the thermal and mechanical properties of the lithosphere. *Journal of Geophysical Research*, 88:4183–4214, 1983.

J. Chorowicz. The East African rift system. *Journal of African Earth Sciences*, 43: 379–410, 2005. doi: 10.1016/j.jafrearsci.2005.07.019.

A. Copley, J.-P. Avouac, and J.-Y. Royer. India-Asia collision and the Cenozoic slowdown of the Indian plate: Implications for the forces driving plate motions. *Journal of Geophysical Research*, 115, 2010. doi: 10.1029/2009JB006634.

D. G. Cornwell, G. D. Mackenzie, R. W. England, P. K. H. Maguire, L. M. Asfaw, and B. Oluma. Northern Main Ethiopian Rift crustal structure from new high-precision gravity data. In *The Afar volcanic province within the East African Rift system*, volume 259, pages 307–321. Geological Society Special Publications, 2006.

D. G. Cornwell, P. K. H. Maguire, R. W. England, and G. W. Stuart. Imaging detailed crustal structure and magmatic intrusion across the Ethiopian Rift using a dense linear broadband array. *Geochemistry, Geophysics, Geosystems*, 11, 2010. doi: 10.1029/2009GC002637.

P. A. Cowie, C. H. Scholz, M. Edwards, and A. Malinverno. Fault Strain and Seismic Coupling on Mid-Ocean Ridges. *Journal of Geophysical Research*, 98:17911–17920, 1993.

A. G. Crosby, S. Fishwick, and N. White. Structure and Evolution of the Intracratonic Congo Basin. *Geochemistry, Geophysics, Geosystems*, 11, 2010. doi: 10.1029/2009GC003014.

M. C. Daly, S. R. Lawrence, K. Dienu-Tshiband, and B. Matouana. Tectonic evolution of the Cuvette Centrale, Zaire. *Journal of the Geological Society, London*, 149:539–546, 1992.

A. Daradich, J. X. Mitrovica, R. N. Pysklywec, S. D. Willett, and A. M. Forte. Mantle flow, dynamic topography, and rift-flank uplift of Arabia. *Geology*, 31:901–904, 2003.

B. De Waele, S. P. Johnson, and S. A. Pisarevsky. Palaeoproterozoic to Neoproterozoic growth and evolution of the eastern Congo Craton: Its role in the Rodinia puzzle. *Precambrian Research*, 160:127–141, 2008. doi: 10.1016/j.precamres.2007.04.020.

B. Deloius, M. Vallée, M. Meghraoui, E. Calais, S. Maouche, K. Lammali, A. Mahsas, P. Briole, F. Benhamouda, and K. Yelles. Slip distribution of the 2003 Boumerdes-Zemmouri earthquake, Algeria, from teleseismic, GPS, and coastal uplift data. *Geophysical Research Letters*, 31, 2004. doi: 10.1029/2004GL020687.

D. Delvaux and A. Barth. African stress pattern from formal inversion of focal mechanism data. *Tectonophysics*, 482:105–128, 2010. doi: 10.1016/j.tecto.2009.05.009.

M. T. Dugda, A. A. Nyblade, J. Julia, C. A. Langston, C. J. Ammon, and S. Simiyu. Crustal structure in Ethiopia and Kenya from receiver function analysis: Implications for rift development in eastern Africa. *Journal of Geophysical Research*, 110, 2005. doi: 10.1029/2004JB003065.

M. T. Dugda, A. A. Nyblade, and J. Julia. Thin Lithosphere Beneath the Ethiopian Plateau Revealed by a Joint Inversion of Rayleigh Wave Group Velocities and Receiver Functions. *Journal of Geophysical Research*, 112, 2007. doi: 10.1029/2006JB004918.

A.M. Dziewonski, T-A. Chou, and J.H. Woodhouse. Determination of earthquake source parameters from waveform data for studies of global and regional seismicity. *J. Geophys. Res.*, 86:2825–2852, 1981.

D. W. Eaton, F. Darbyshire, R. L. Evans, H. Grütter, A. G. Jones, and X. Yuan. The elusive lithosphere-asthenosphere boundary (LAB) beneath cratons. *Lithos*, 109:1–22, 2009. doi: 10.1016/j.lithos.2008.05.009.

C. Ebinger, Y. Poudjom Djomani, E. Mbede, A. Foster, and J. B. Dawson. Rifting Archean lithosphere: the Eyasi-Manyara-Natron rifts, East Africa. *Journal of the Geological Society*, 154:947–960, 1997.

C. J. Ebinger and N. H. Sleep. Cenozoic magmatism throughout east Africa resulting from impact of a single plume. *Nature*, 395:788–791, 1998. doi: 10.1038/27417.

C. J. Ebinger, J. A. Jackson, A. N. Foster, and N. J. Hayward. Extensional basin geometry and the elastic lithosphere. *Philosophical Transactions of the Royal Society of London*, 357:741–765, 1999.

B. Emmerson and D. M^{c}Kenzie. Thermal structure and seismicity of subducting lithosphere. *Physics of the Earth and Planetary Interiors*, 163:191–208, 2007. doi: 10.1016/j.pepi.2007.05.007.

E. R. Engdahl and A. Villaseñor. Global Seismicity 1900-1999. In W. H. K. Lee, H. Kanamori, P. C. Jennings, and C. O. Kisslinger, editors, *International Handbook of Earthquake and Engineering Seismology*, volume 81A, chapter 41, pages 665–690. Academic Press, 2002.

E.R. Engdahl, R.D. van der Hilst, and R.P. Buland. Global teleseismic earthquake relocation with improved travel times and prceedures for depth determination. *Bulletin of the Seismological Society of America*, 88:722–743, 1998.

P. C. England and A. B. Thompson. Pressure-temperature-time paths of regional metamorphism I. Heat transfer during evolution of regions of thickened continental crust. *Journal of Petrology*, 25:894–928, 1984.

A. Foster, C. Ebinger, M. Mbede, and D. Rex. Tectonic development of the northern Tanzanian sector of the East African Rift. *Journal of the Geological Society of London*, 154:689–700, 1997.

A. N. Foster and J. A. Jackson. Source paramters of large African earthquakes: implications for crustal rheology and regional kinematics. *Geophysical Journal International*, 134:422–448, 1998.

T. Furman. Geochemistry of East African Rift basalts: An overview. *Journal of African Earth Sciences*, 48:147–160, 2007. doi: 10.1016/j.jafrearsci.2006.06.009.

T. Furman. Melting of metasomatized subcontinental lithosphere: undersaturated mafic lavas from Rungwe, Tanzania. *Contributions to Mineralogy and Petrology*, 122:97–115, 1995.

R. Gaulon, J. Chorowicz, G. Vidal, B. Romanowicz, and G. Roult. Regional geodynamic implications of the May-July 1990 earthquake sequence in southern Sudan. *Tectonophysics*, 209:87–103, 1992.

A. Ghosh, W. E. Holt, and L. M. Flesch. Contribution of gravitational potential energy differences to the global stress field. *Journal of Geophysical Research*, 179:787–812, 2009. doi: 10.1111/j.1365-246X.2009.04326.x.

N. L. Grimison and W.-P. Chen. Earthquakes in the Davie Ridge-Madagascar Region and the Southern Nubian-Somalian Plate Boundary. *Journal of Geophysical Research*, 93:10439–10450, 1988a.

N. L. Grimison and W.-P. Chen. Source mechanisms of four recent earthquakes along the Azores-Gibralter plate boundary. *Geophysical Journal*, 92:391–401, 1988b.

H. Grütter, D. Latti, and A. Menzies. Cr-Saturation Arrays in Concentrate Garnet Compositions from Kimberlite and their Use in Mantle Barometry. *Journal of Petrology*, 47:801–820, 2006.

L. Hagos, H. Shomali, and R. Roberts. Re-evaluation of focal depths and source mechanisms of selected earthquakes in the Afar depression. *Geophysical Journal International*, 167:297–308, 2006. doi: 10.1111/j.1365-246X.2006.03091.x.

R. Hartley and P. A. Allen. Interior cratonic basins of Africa: relation to continental break-up and role of mantle convection. *Basin Research*, 6:95–113, 1996.

R. Hartley, A. B. Watts, and J. D. Fairhead. Isostacy of Africa. *Earth and Planetary Science Letters*, 137:1–18, 1966.

D. Hatzfeld and M. Frogneux. Intermediate depth seismicity in the western Mediterranean unrelated to subduction of oceanic lithosphere. *Nature*, 292:443–445, 1981.

D. B. Hendrie, N. J. Kusnir, C. K. Morley, and C. J. Ebinger. Cenozoic extension in northern Kenya: a quantitative model of rift basin development in the Turkana region. *Tectonophysics*, 236:409–438, 1994.

R. Hofstetter and M. Beyth. The Afar Depression: interpretation of the 1960-2000 earthquakes. *Geophyscial Journal International*, 155:715–732, 2003.

P. Y. Huang and S. C. Solomon. Centroid Depths and Mechanisms of Mid-Ocean Ridge Earthquakes in the Indian, Gulf of Aden, and Red Sea. *Journal of Geophysical Research*, 92:1361–1382, 1987.

M. Ibs-von Seht, S. Blumenstein, R. Wagner, D. Hollnack, and J. Wohlenberg. Seismicity, seismotectonics and crustal structure of the southern Kenya Rift - new data from the Lake Magadi area. *Geophysical Journal International*, 146:439–453, 2001. doi: 10.1046/j.0956-540X.2001.01464.x.

J. Jackson and T. Blenkinsop. The Malawi earthquake of March 10, 1989: Deep faulting within the East African Rift System. *Tectonics*, 12:1131–1139, 1993.

J. Jackson and T. Blenkinsop. The Bilila-Mtakataka fault in Malawi: An active, 100-km long normal fault segment in thick seismogenic crust. *Tectonics*, 16:137–150, 1997.

J. Jackson, D. M^{c}Kenzie, K. Priestley, and B. Emmerson. New views on the structure and rheology of the lithosphere. *Journal of the Geological Society, London*, 165: 453–465, 2008. doi: 10.1144/0016-76492007-109.

J. A. Jackson and N. J. White. Normal faulting in the upper continental crust: observations from regions of active extension. *Journal of Structural Geology*, 11:15–36, 1989.

J. A. Jackson, N. J. White, Z. Garfunkel, and H. Anderson. Relations between normal-fault geometry, tilting and vertical motions in extensional terrains: an example from the southern Gulf of Suez. *Journal of Structural Geology*, 10:155–170, 1988.

J. A. Jackson, H. Austrheim, D. M^{c}Kenzie, and K. Priestley. Metastability, mechanical strength, and the support of mountain belts. *Geology*, 32:625–628, 2004. doi: 10.1130/G20397.1.

E. Jacques, J. C. Ruegg, J. C. Lépine, P. Tapponnier, and G. C. P. King. Relocation of M $\geq$ 2 events of the 1989 Dôbi seismic sequence in Afar: evidence for earthquake migration. *Geophysical Journal Internation*, 138:447–469, 1999.

D. Keir, C. J. Ebinger, G. W. Stuart, E. Daly, and A. Ayele. Strain accomodation by magmatism and faulting as rifting proceeds to breakup: Seismicity of the northern Ethiopian rift. *Journal of Geophysical Research*, 111, 2006. doi: 10.1029/2005JB003748.

D. Keir, I. D. Bastow, K. A. Whaler, E. Daly, D. G. Cornwall, and S. Hautot. Lower crustal earthquakes near the Ethiopian rift induced by magmatic processes. *Geochemistry, Geophysics, Geosystems*, 10, 2009. doi: 10.1029/2009GC002382.

B. L. N. Kennett, E. R. Engdahl, and R. Buland. Constraints on seismic velocities in the Earth from travel times. *Geophysical Journal International*, 122:108–124, 1995.

G. Laske and T. G. Masters. A gobal digital map of sediment thickness. *EOS. Transactions AGU 78*, F483:see http://mahi.ucsd.edu/Gabi/sediment.html, 1997.

R. J. Last, A. A. Nyblade, and C. A. Langston. Crustal structure of the East African Plateau from receiver functions and Rayleigh wave phase velocities. *Journal of Geophysical Research*, 102:24469–24483, 1997.

X. Le Pichon, P. Henry, and B. Goffé. Uplift of Tibet: from eclogites to granulites - implications for the Andean Plateau and the Variscan belt. *Tectonophysics*, 273: 57–76, 1997.

J.-C. Lépine and A. Hirn. Seismotectonics on the Republic of Djibouti, linking the Afar Depression and the Gulf of Aden. *Tectonophysics*, 209:65–86, 1992.

J. P. Liégeois, A. Benhallou, A. A. Azzouni-Sekkal, R. Yahiaoui, and B. Bonin. The Hoggar swell and volcanism: Reactivation of the Precambrian Tuareg shield during Alpine convergence and West African Cenozoic volcanism. *Geological Society of America, Special Paper*, 388, 2005. doi: 10.1130/2005.2388(23).

L. Lonergan and N. White. Origin of the Betic-Rif mountain belt. *Tectonics*, 16: 504–522, 1997.

M. G. Lund, H. Austrheim, and M. Erambert. Earthquakes in the deep continental crust - insights from studies on exhumed high-pressure rocks. *Geophysical Journal International*, 158:569–576, 2004. doi: 10.1111/j.1365-246X.2004.02368.x.

G. D. Mackenzie, H. Thybo, and P. K. H. Maguire. Crustal velocity structure across the Main Ethiopian Rift: results from two-dimensional wide-angle seismic modelling. *Geophysical Journal International*, 162:994–1006, 2005. doi: 10.1111/j.1365-246X.2005.02710.x.

A. Maggi, J. A. Jackson, D. M^{c}Kenzie, and K. Priestley. Earthquake focal depths, effective elastic thickness, and the strength of the continental lithosphere. *Geology*, 28:495–498, 2000.

P. K. H. Maguire, G. R. Keller, S. L. Klemperer, G. D. Mackenzie, K. Keranen, S. Hardler, B. O'Reilly, H. Thybo, L. Asfaw, M. A. Khan, and M. Amha. Rifting in the Afar volcanic province: Geophysical studies of crustal structure and processes. *Geological Society Special Publications*, 259:269–282, 2006.

R. McCaffrey and G. Abers. SYN3: A program for inversion of teleseismic waveforms on microcomputers, Air Force Geophysics Laboratory Technical Report AFGL-TR-0099. Technical report, Hansomb Air Force Base, Massachusetts, 1988.

R. McCaffrey, P. Zwick, and G. Abers. SYN4 program. *IASPEI Sofware Library*, 3: 81–166, 1991.

D. M^{c}Kenzie. Estimating T_e in the presence of internal loads. *Journal of Geophysical Research*, 108:doi:10.1029/2002JB001766, 2003.

D. M^{c}Kenzie. The influence of dynamically supported topography on estimates of T_e. *Earth and Planetary Sciences*, 295:127–138, 2010. doi: 10.1016/j.epsl.2010.03.033.

D. M^{c}Kenzie. Some remarks on the movement of small melt fractions in the mantle. *Earth and Planetary Sciences Letters*, 95:53–72, 1989.

D. M^{c}Kenzie and D. Fairhead. Estimates of the effective elastic thickness of the continental lithosphere from Bouguer and free air gravity anomalies. *Journal of Geophysical Research*, 102:27523–27552, 1997.

D. M^{c}Kenzie and K. Priestley. The influence of lithospheric thickness variations on continental evolution. *Lithos*, 102:1–11, 2008. doi: 10.1016/j.lithos.2007.05.005.

D. M^{c}Kenzie, J. Jackson, and K. Priestley. Thermal structure of oceanic and continental lithosphere. *Earth and Planetary Science Letters*, 233:337–349, 2005. doi: 10.1016/j.epsl.2005.02.005.

J. G. Meert. A synopsis of events related to the assembly of eastern Gondwana. *Tectonophysics*, 362:1–40, 2003. doi: 10.1016/S0040-1951(02)00629-7.

P. Molnar and H. Lyon-Caen. Fault plane solutions of earthquakes and active tectonics of the Tibetan Plateau and its margins. *Geophys. J. Int.*, 99:123–153, 1989.

R. D. Muller, M. Sdrolias, C. Gaina, and W. R. Roest. Age, spreading rates, and spreading asymmetry of the world's ocean crust. *Geochemistry, Geophysics, Geosystems*, 9, 2008. doi: 10.1029/2007GC001743.

J. Nábělek. *Determination of earthquake source parameters from inversion of body waves*. PhD thesis, Massachusetts Institute of Technology, 1984a.

J. Nábělek. Geometry and mechanism of faulting of the 1980 El Asnam, Algeria, Earthquake from inversion of teleseismic body waves and comparison with field observations. *Journal of Geophysical Research*, 90:12713–12728, 1984b.

S. K. Nair, S. S. Gao, K. H. Liu, and P. G. Silver. Southern African crustal evolution and composition: Constraints from receiver function studies. *Journal of Geophysical Research*, 111, 2006. doi: 10.1029/2005JB003802.

A. E. M. Narin, I. Lerche, and J. E. Iliffe. Geology, basin analysis and hydrocarbon potential of Mozambique and the Mozambique Channel. *Earth Science Reviews*, 30: 81–124, 1991.

T. K. Nguuri, J. Gore, D. E. James, S. J. Webb, C. Wright, T. G. Zengeni, O. Gwavava, J. A. Snoke, and Kaapvaal Seismic Group. Crustal structure beneath southern Africa and its implications for the formation and evolution of the Kaapvaal and Zimbabwe cratons. *Geophysical Research Letters*, 28:2501–2504, 2001. doi: 10.1029/2000GL012587.

O. Nilsen, E. Hagen, and H. Dypvik. Sediment provenance and Karoo rift basin evolution in the Kilombero Rift Valley, Tanzania. *South African Journal of Geology*, 104: 137–150, 2001.

A. A. Nyblade and R. A. Brazier. Precambrian lithospheric controls on the development of the East African rift system. *Geology*, 30:755–758, 2002. doi: 10.1130/0091-7613(2002)030.

A. A. Nyblade and C. A. Langston. East African earthquakes below 20km depth and their implications for crustal structure. *Geophysical Journal International*, 121:49–62, 1995.

A. A. Nyblade and S. W. Robinson. The African Superswell. *Geophysical Research Letters*, 21:765–768, 1994.

A. A. Nyblade, C. Birt, C. A. Langston, T. J. Owens, and R. J. Last. Seismic Experiment Reveals Rifting of Craton in Tanzania. *Eos, Transactions*, 77:517–521, 1996a.

A. A. Nyblade, K. S. Vogfjord, and C. A. Langston. P wave velocity of Proterozoic upper mantle beneath central and southern Africa. *Journal of Geophysical Research*, 101:11159–11171, 1996b.

A. A. Nyblade, T. J. Owens, H. Gurrola, J. Ritsema, and C. A. Langston. Seismic evidence for a deep upper mantle thermal anomaly beneath east Africa. *Geology*, 28: 599–602, 2000.

J. S. Pallister, W. A. McCausland, S. Jónsson, Z. Lu, H. M. Zahran, S. El Hadidy, A. Aburukbah, I. C. F. Stewart, P. R. Lundgren, R. A. White, and M. R. H. Moufti. Broad accomodation of rift-related extension recorded by dyke intrusion in Saudi Arabia. *Nature Geoscience*, 3, 2010. doi: 10.1038/NGEO966.

B. Parsons and F. M. Richter. A relation between the driving force and geoid anomaly associated with mid-ocean ridges. *Earth and Planetary Science Letters*, 51:445–450, 1980.

N. K. Pavlis, S. A. Holmes, S. C. Kenyon, and J. K. Factor. An Earth gravitational model to degree 2160: EGM2008. In *2008 General Assembly of the European Geosciences Union*, Vienna, Austria, April 2008.

M. Pérez-Gussinyé, M. Metois, M. Fernández, J. Vergés, J. Fullea, and A. R. Lowry. Effective elastic thickness of Africa and its relationship to other proxies for lithospheric structure and surface tectonics. *Earth and Planetary Science Letters*, 287:152–167, 2009. doi: 10.1016/j.epsl.2009.08.004.

H. Porada. Pan-African Rifting and Orogensis in Southern to Equatorial Africa and Eastern Brazil. *Precambrian Research*, 44:103–136, 1989.

K. Priestley and D. McKenzie. The thermal structure of the lithosphere from shear wave velocities. *Earth and Planetary Science Letters*, 244:285–301, 2006. doi: 10.1016/j.epsl.2006.01.008.

K. Priestley, D. McKenzie, E. Debayle, and S. Pilidou. The African upper mantle and its relationship to tectonics and surface geology. *Geophys. J. Int.*, 175:1108–1126, 2008. doi: 10.1111/j.1365-246X.2008.03951.x.

C. Prodehl, A. W. B. Jacobs, E. Thybo, E. Dindi, and R. Stangl. Crustal structure on the northeastern flank of the Kenya rift. *Tectonophysics*, 236:271–290, 1994.

C. Prodehl, J. R. R. Ritter, J. Mechie, G. R. Keller, M. A. Khan, B. Jacob, K. Fuchs, I. O. Nyambok, J. D. Obel, and D. Riaroh. The KRISP 94 lithospheric investigation of southern Kenya — the experiments and the main results. *Tectonophysics*, 278: 121–147, 1997.

M. Reyners, D. Eberhart-Phillips, and G. Stuart. The role of fluids in lower-crustal earthquakes near continental rifts. *Nature*, 446:1075–1078, 2007. doi: 10.1038/nature05743.

R. M. Richardson. Ridge forces, absolute plate motions and the intraplate stress field. *Journal of Geophysical Research*, 97:11739–11748, 1992.

U. Ring. The influence of preexisting structure on the evolution of the Cenozoic Malawi rift (East African rift system). *Tectonics*, 13:313–326, 1994.

B. R. Rosendahl, E. Kilembe, and K. Kaczmarick. Comparison of the Tanganyika, Malawi, Rukwa and Turkana Rift zones from analyses of seismic reflection data. *Tectonophysics*, 213:235–256, 1992.

R. L. Rudnick and D. M. Fountain. Nature and composition of the continental crust: A lower crustal perspective. *Reviews of Geophysics*, 33,3:267–309, 1995.

D. V. Rundquist and P. O. Sobolev. Seismicity of mid-ocean ridges and its geodynamic implications: a review. *Earth-Science Reviews*, 58:143–161, 2002. doi: 10.1016/S0012-8252(01)00086-1.

C. H. Scholz. *The Mechanics of Earthquakes and Faulting*. Cambridge University Press, 2nd edition, 2002.

C. H. Scholz and J. C. Contreras. Mechanics of continental rift architecture. *Geology*, 26:967–970, 1998.

T. Seno and A. Saito. Recent East African earthquakes in the lower crust. *Earth and Planetary Science Letters*, 121:125–136, 1994.

B. Shaw and J. Jackson. Earthquake mechanisms and active tectonics of the Hellenic subduction zone. *Geophysical Journal International*, 181:966–984, 2010. doi: 10.1111/j.1365-246X.2010.04551.x.

G. N. Shudofsky. Source mechanisms and focal depths of East African earthquakes using Rayleigh-wave inversion and body-wave modelling. *Geophysical Journal of the Royal Astronomical Society*, 83:563–614, 1985.

G. N. Shudofsky, S. Cloetingh, S. Stein, and R. Wortel. Unusually deep earthquakes in East Africa: constraints on the thermo-mechanical structure of a continental rift system. *Geophysical Research Letters*, 14:741–744, 1987.

H. Soosalu, J. Key, R. S. White, C. Knox, P. Einarsson, and S. S. Jakobsdóttir. Lower-crustal earthquakes caused by magma movement beneath Askja volcano on the north Iceland Rift. *Bulletin of Volcanology*, 72, 2009. doi: 10.1007/s00445-009-0297-3.

D. S. Stamps, E. Calais, E. Saria, C. Hartnady, J.-M. Nocquet, C. J. Ebinger, and R. M. Fernandes. A kinematic model for the East African Rift. *Geophysical Research Letters*, 35, 2008. doi: 10.1029/2007GL032781.

D. S. Stamps, L. M. Flesch, and E. Calais. Lithospheric bouyancy forces in Africa from a thin sheet approach. *International Journal of Earth Sciences*, 2010. doi: 10.1007/s00531-010-0533-2.

K. M. Tainton, A. G. Seggie, B. A. Bayley, I. Tomlinson, and K. E. Quadling. Garnet Thermobarometry: Implications for Mantle Heat Flow within the Tanzanian Craton. In J. J. Gurney, J. L Gurney, M. D. Pascoe, and S. H. Richardson, editors, *Proceedings of the 7th international Kimberlite conference*, pages 852–860, Red Roof Design, Cape Town, 1999.

T. Taymaz, J. Jackson, and R. Westaway. Earthquake mechanisms in the Hellenic trench near Crete. *Geophys. J. Int.*, 102:424–443, 1990.

F. A. Tugume and A. A. Nyblade. The depth distribution of seismicity at the northern end of the Rwenzori mountains: Implications for heat flow in the western branch of the East African Rift System in Uganda. *South African Journal of Geology*, 112: 261–276, 2009.

E. Vittori, D. Delvaux, and F. Kervyn. Kanda fault: a major seismogenic element west of the Rukwa rift (Tanzania, East Africa). *Journal of Geodynamics*, 24:139–153, 1997.

D. S. Weeraratne, D. W. Forsyth, K. M. Fischer, and A. A. Nyblade. Evidence for an upper mantle plume beneath the Tanzanian craton from Rayleigh wave tomography. *Journal of Geophysical Research*, 108, 2003.

P. Wessel and W.H.F. Smith. New, improved version of Generic Mapping Tools released. *Eos Trans AGU*, 79, 1998.

R. Westaway. Forces associated with mantle plumes. *Earth and Planetary Science Letters*, 119:331–348, 1993.

R. Wortel. Deep earthquakes and the thermal assimilation of subducting lithosphere. *Geophysical Research Letters*, 13:34–37, 1986.

T. J. Wright, C. Ebinger, J. Biggs, A. Ayele, G. Yirgu, D. Keir, and A. Stork. Magma-maintained rift segmentation at continental rupture in the 2005 Afar dyking episode. *Nature*, 442:291–294, 2006. doi: 10.1038/nature04978.

T. L. Wright and F. W. Klein. Deep magma transport at Kilauea volcano, Hawaii. *Lithos*, 87:50–79, 2006. doi: 10.1016/j.lithos.2005.05.004.

Z. Yang and W.-P. Chen. Mozambique earthquake sequence of 2006: High-Angle normal faulting in southern Africa. *Journal of Geophysical Research*, 113, 2008.

Z. Yang and W.-P. Chen. Earthquakes along the East African Rift System: A multi-scale, system-wide perspective. *Journal of Geophysical Research*, 115, 2010. doi: 10.1029/2009JB006779.

B. W. D. Yardley. The role of water in the evolution of the continental crust. *Journal of the Geological Society of London*, 166:585–600, 2009. doi: 10.1144/0016-76492008-101.

P. A. V. Young, P. K. H. Maguire, N. d'A. Laffoley, and J. R. Evans. Implications of the distribution of seismicity near Lake Bogoria in the Kenya rift. *Geophysical Journal International*, 105:665–674, 1991.

P. Zwick, R. McCaffrey, and G. Abers. MT5 program. *IASPEI Software Library*, 4, 1994.

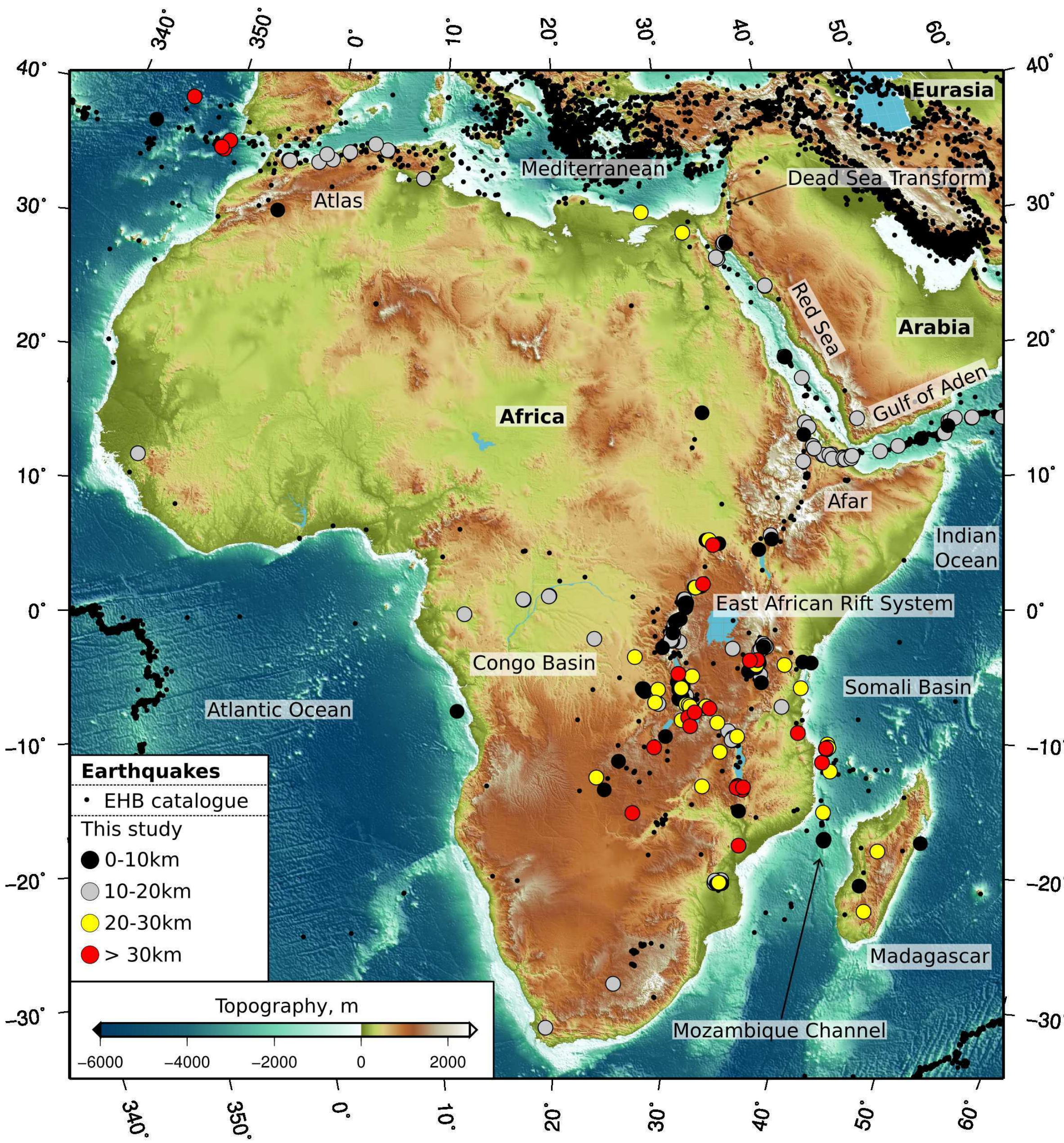

Figure 1: Seismicity in Africa. Small black dots show the full EHB catalogue, updated from Engdahl et al. (1998). Coloured dots are events constrained by body waveform or depth phase modelling, used in this study. Topography is from the SRTM30PLUS model (Becker et al., 2009). The topographic scale given applies to this and all subsequent figures. The principle geographic features are labeled.

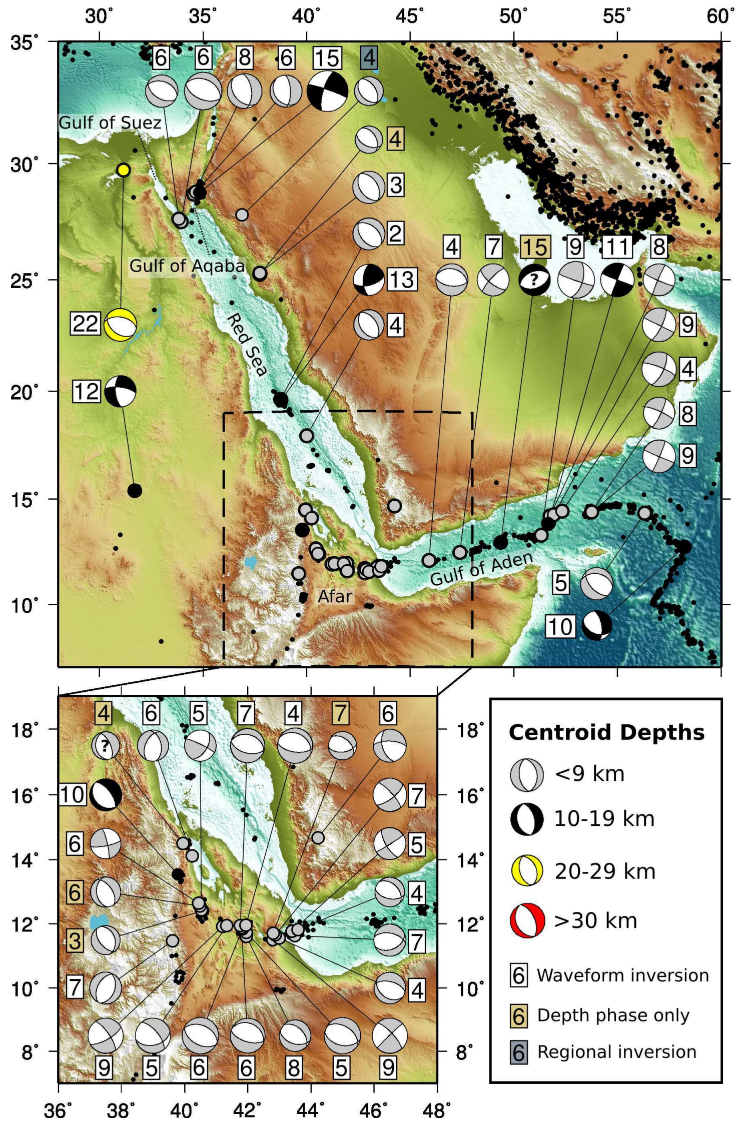

Figure 2: Seismicity along the Africa-Arabia margin. Topography scale in this and subsequent figures is as in Figure 1. For focal mechanisms, shaded quadrants are compressional, white quadrants are dilatational, with the shading indicative of the event depth. Grey events are $\leq$9 km, black are 10-19 km, yellow are 20-29 km, red are $\geq$30 km. Depth is also given by the number adjacent to each mechanism. All depths are for centroids in km. Due to the density of events in Afar, the region is provided as an inset.

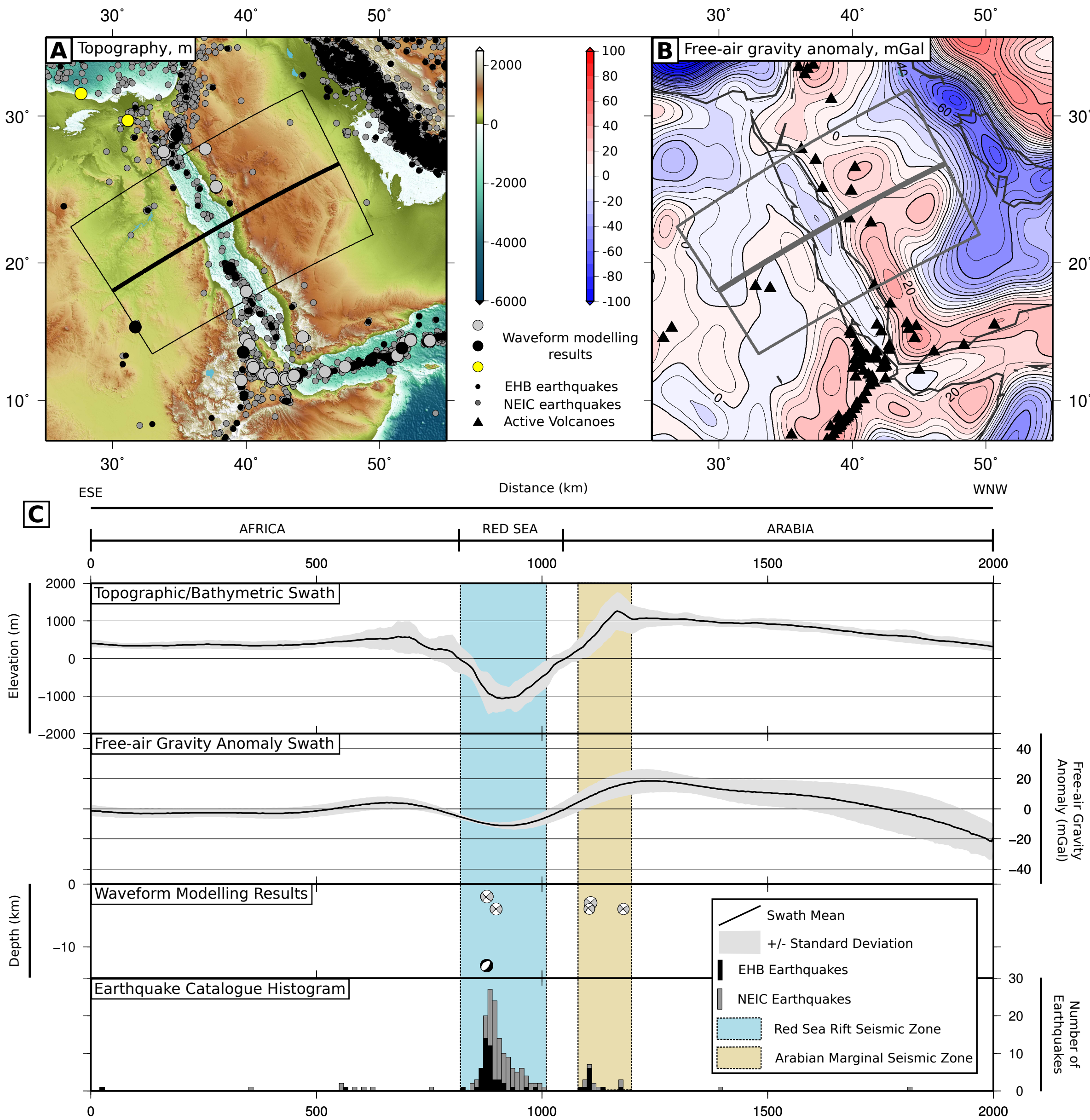

Figure 3: (a) Topography and (b) Free-air gravity anomalies for the Red Sea and its margins. Circles represent earthquakes. Black triangles are areas of active volcanism, from the Smithsonian Global Volcanism Catalogue. The outlined areas are the areas for the swaths presented in (c), with the centre line, and line of projection for earthquakes in (c) shown by the thicker line. (c) Topographic swath and free-air gravity anomaly swath for the grey box in (a) and (b). Waveform modelling results, and earthquake frequency histogram, based on the EHB and NEIC catalogues, for the same area, projected onto the line through the centre of the swath area. Blue box highlights the region of activity related to the oceanic spreading centre in the Red Sea. Yellow area highlights the area of increased seismic activity along the Arabian margin.

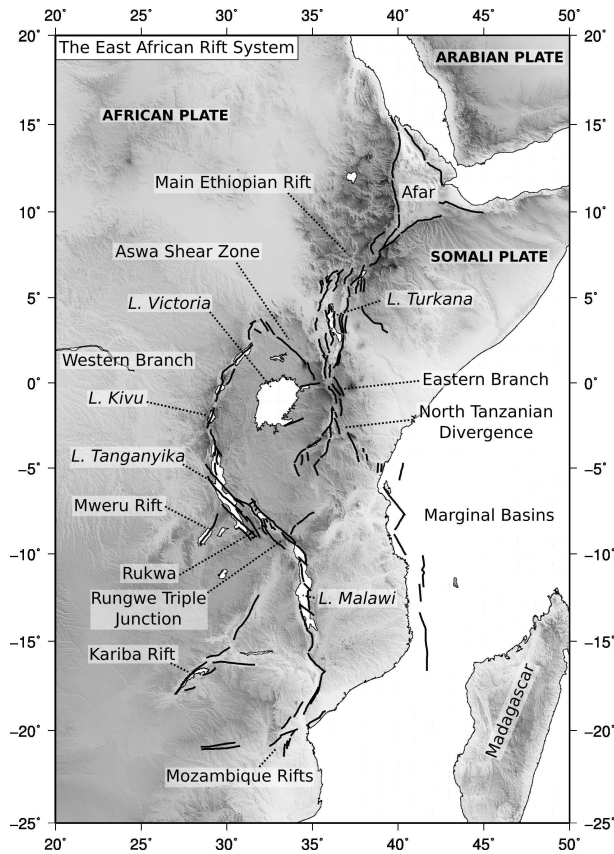

Figure 4: The East African Rift System. Major active faults, from Chorowicz (2005) are shown as black lines. Extension across the region is principally WNW-ESE (Stamps et al., 2008).

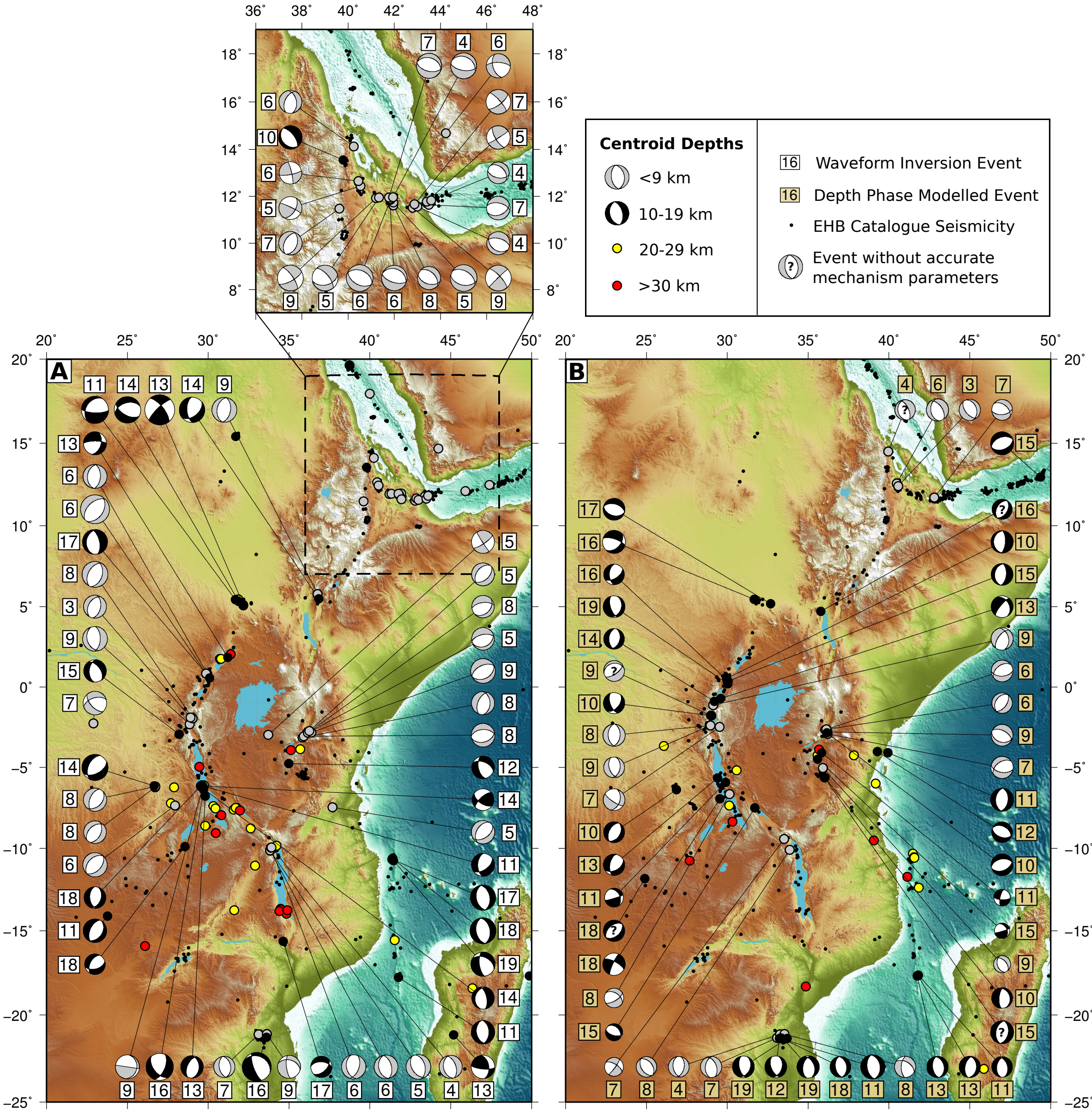

Figure 5: Earthquakes along the East African Rift with centroids < 20 km. (a) Source parameters for earthquakes determined from body waveform modelling. The Afar region is shown inset. (b) Earthquakes depths determined from forward modelling of depth phases, plotted using the gCMT mechanisms. No gCMT mechanism was available for the event marked by a **?**, so a mechanism consistent with available data was assumed for depth-phase modelling. For earthquakes prior to 2009, EHB locations are used. For those occurring in 2009 and 2010, NEIC locations are used. Shading is indicative of centroid depth. All earthquakes from the EHB catalogue are plotted as small black points, geographic location only.

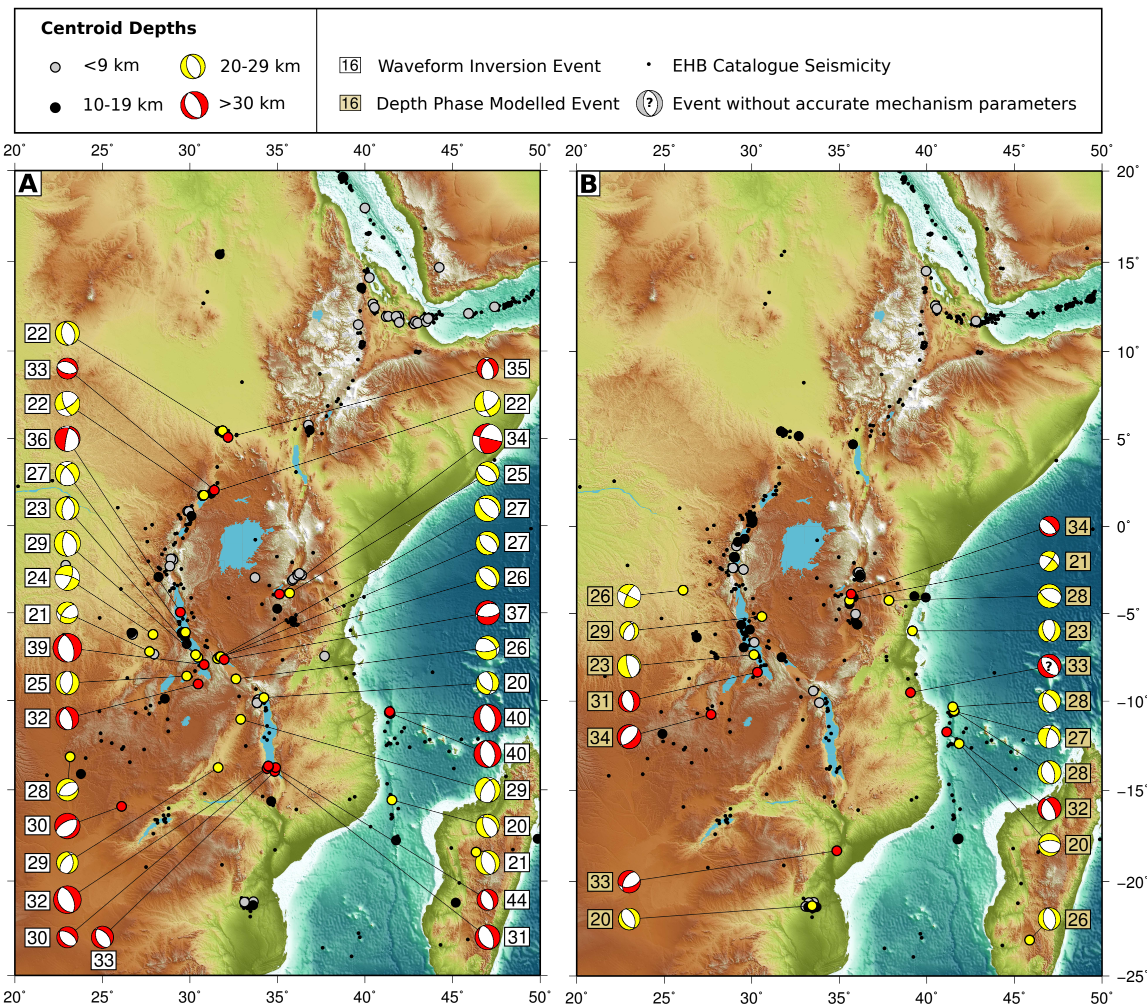

Figure 6: Earthquakes along the East African Rift with centroids $\geq$ 20 km. Caption as for Figure 5.

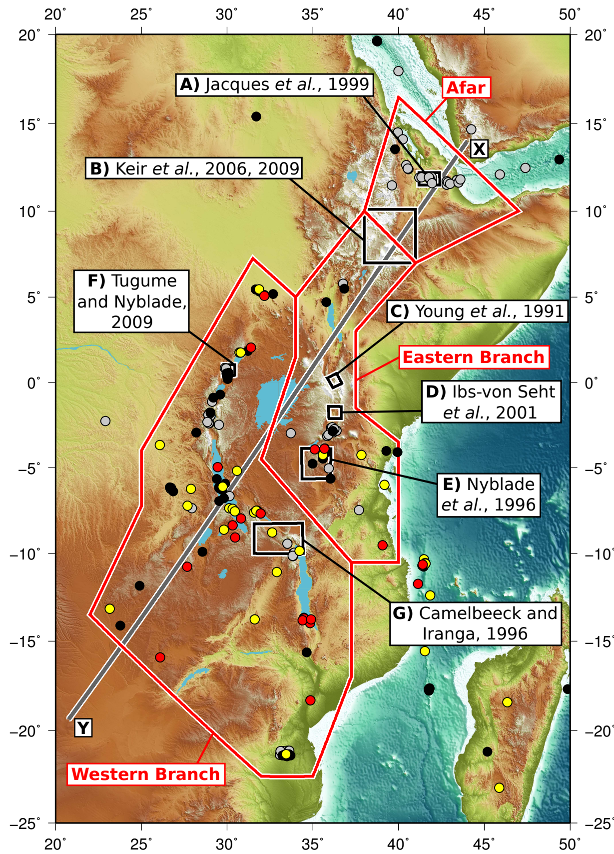

Figure 7: The East African Rift System. The areas of local seismic networks, discussed in the text, are shown by labelled black boxes. Red boxes show the areas of depth/frequency histograms in Figure 8. Grey line shows the line of projection for Figure 10. Earthquake modelling results are shown by coloured circles. Shading is indicative of centroid depth.

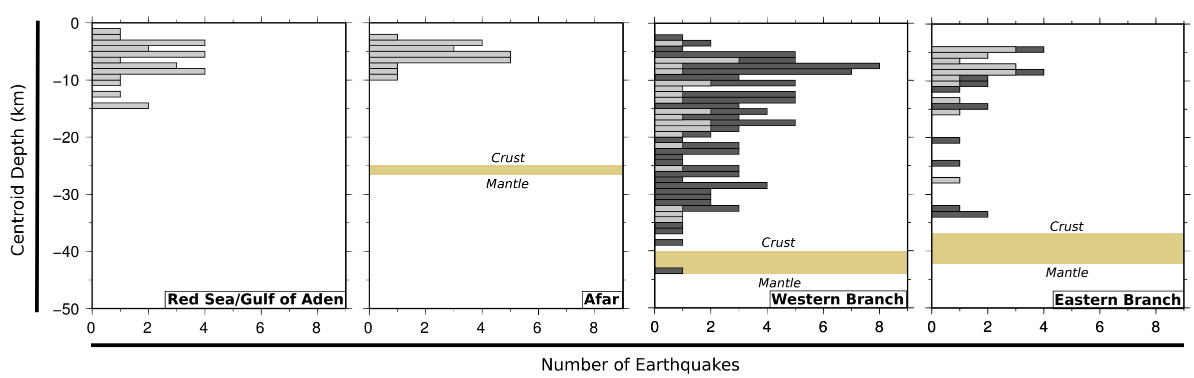

Figure 8: Regional depth/frequency histograms, based on the areas shown in Figure 7. Dark grey events are those occurring in regions with basement ages of Proterozoic or older, lighter grey events occur in regions with basement ages during the Pan-African (Figure 9a). Moho boundaries are taken from Dugda et al. (2005), averaged over the region for which each histogram is plotted.

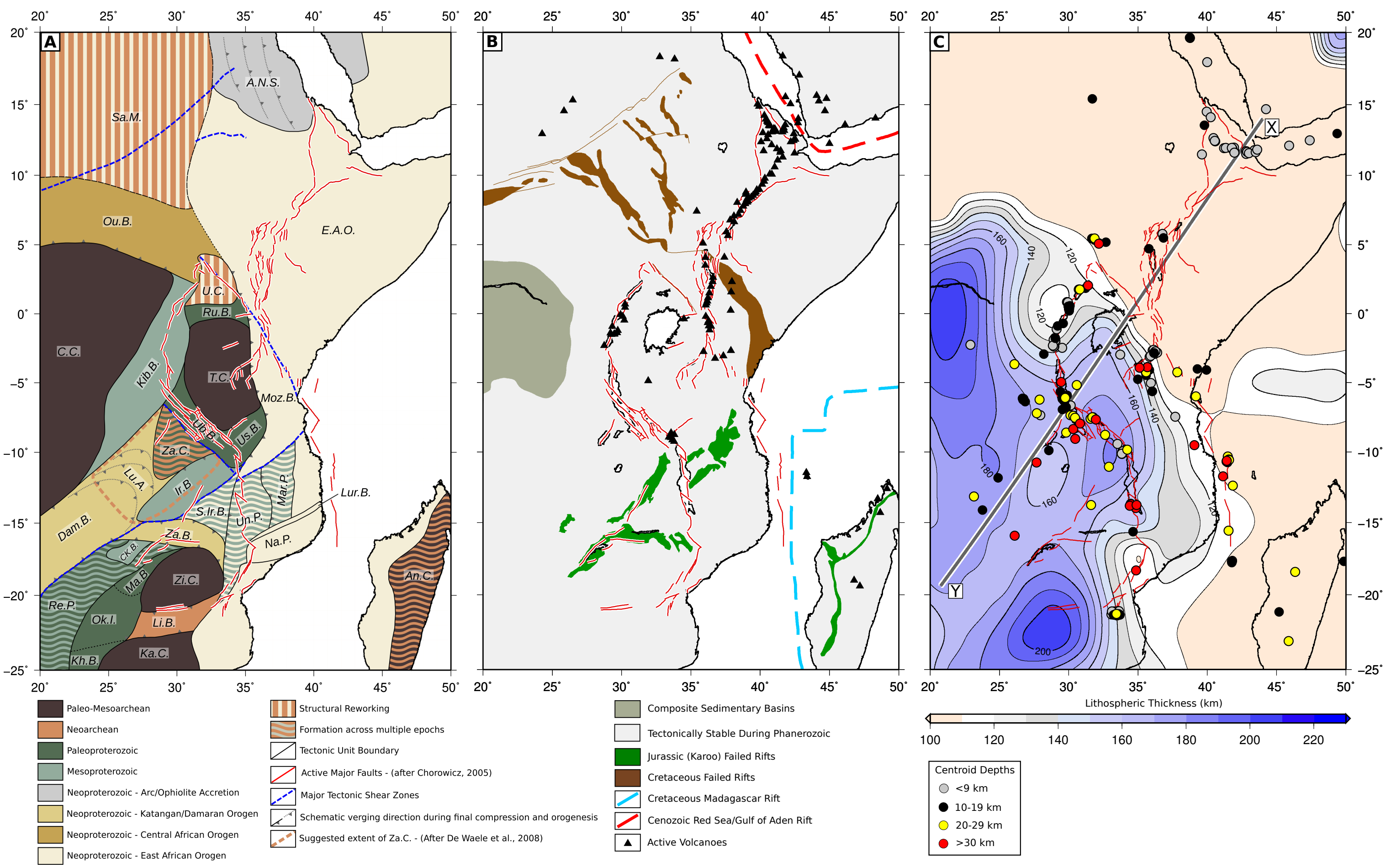

Figure 9: (a) Tectonic architecture of the East African basement. Zi.C. - Zimbabwe Craton, C.C. - Congo Craton, T.C. - Tanzanian Craton, An.C. - Antanarivo Craton, Ka.C. - Kaapvaal Craton, Li.B. - Limpopo Belt, Za.C. - Zambia Craton, Sa.M. - Saharan Metacraton, U.C. - Uganda Craton, Ma.B. - Magondi Belt, Ok.I. - Okwa Inlier, Kh.B. - Kheis Belt, Ub.B. - Ubendian Belt, Us.B. - Usagaran Belt, Ru.B. - Ruwenzori Belt, Re.P. - Rehoboth Province, CK.B. - Choma-Kalomo Block, Kib.B. - Kibaran Belt, Ir.B. - Irumide Belt, S.Ir.B. - Southern Irumide Belt, Un.P. - Unango Province, Mar.P. - Marrupa Province, A.N.S. - Arabian-Nubian Shield, E.A.O. - East African Orogen, Lu.A. - Lufilian Arc, Dam. B. - Damara Belt, Za.B. - Zambezi Belt, Na.P. - Nampula Province, Lur.B. - Lurio Belt. Major active fault lines are included for reference to modern structure. (b) Phanerozoic Tectonics of East Africa. The margins of Africa have all been affected by rifting during the Phanerozoic. Active volcanoes are taken from the Smithsonian Global Volcanism Catalogue. (c) Lithospheric thickness of East Africa, updated from Priestley and M^{c}Kenzie (2006). Earthquakes from this study are included as points, with colour indicating centroid depth. Active fault systems are marked. Grey line from X to Y indicates the line of section for Figure 10.

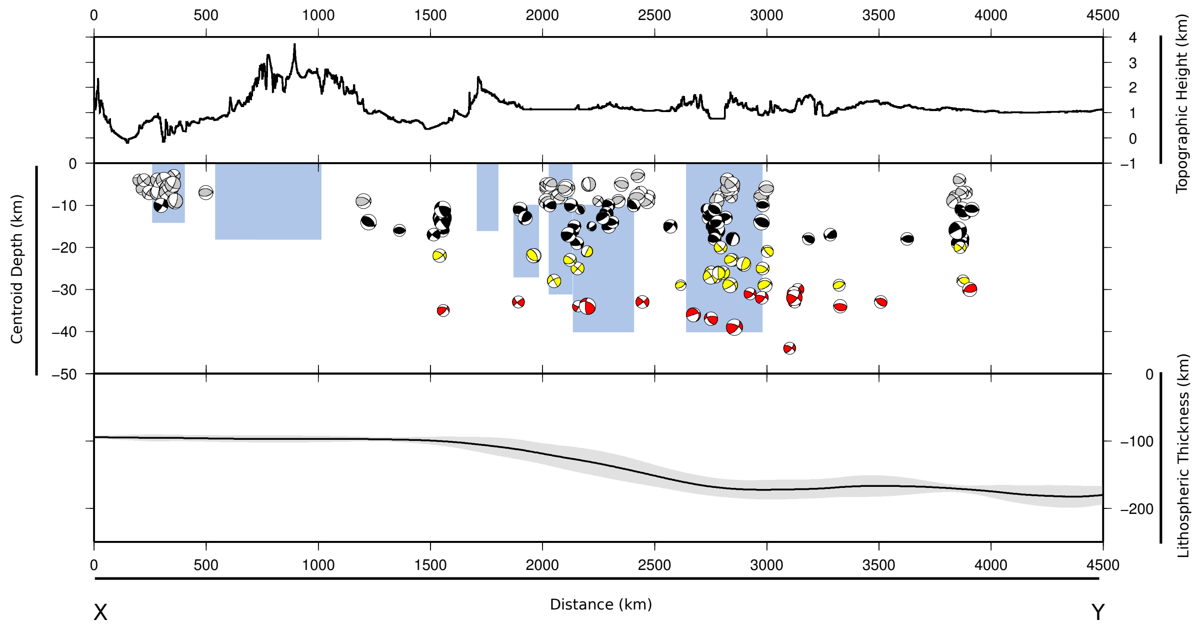

Figure 10: Cross Section taken N-S along the grey line in Figures 7 and 9c. Top panel is topography. Central panel shows focal mechanisms as east-hemisphere projections at locations based on profile-perpendicular projection, plotted at the centroid depths. Colour scheme for the shading of dilatational quadrants is as in Figure 5,6. Only events occurring within the confines of the coastline are plotted. Blue boxes are the areas of the local network studies shown in Figure 7, between the maximum and minimum depth at which earthquakes were determined during the duration of the network. For the study of Keir et al. (2006), we exclude those events related to fluid migration. Bottom panel is a swath track of lithospheric thickness, taken within ±1000 km of the line shown in Figure 9c. Black line represents the mean, grey area is $\pm\sigma$ from the mean.

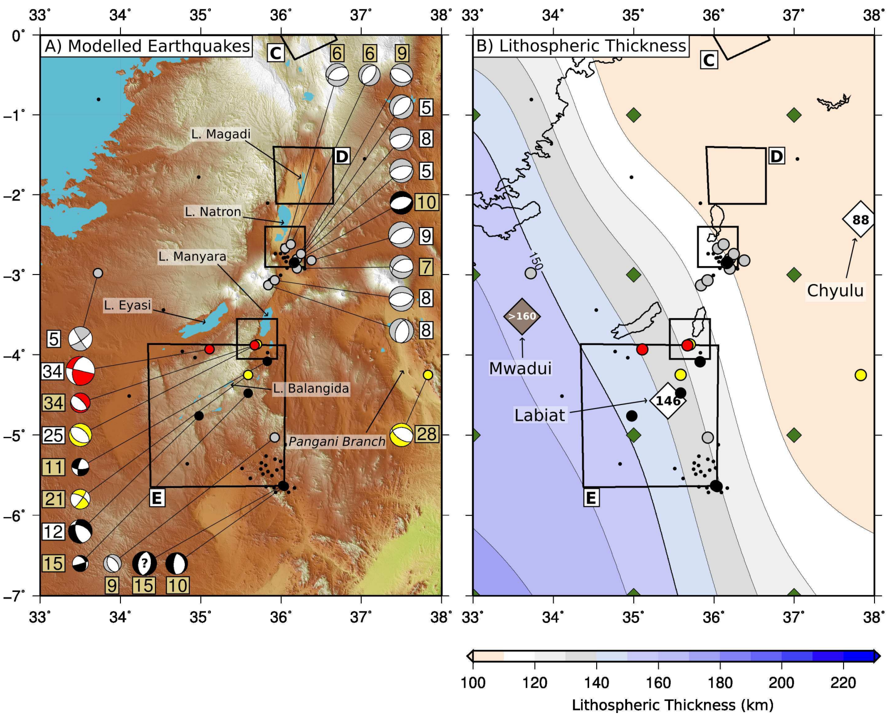

Figure 11: (a) Seismic activity in the North Tanzanian Divergence. Earthquake symbols are as in Figures 5,6. (b) Lithospheric thickness in North Tanzania. Earthquake centroid depths are plotted as points, with colour indicating depth. Green diamonds indicate points where lithospheric thickness is determined from 1D temperature profiles by the method of Priestley et al. (2008). White diamonds are the locations of non-diamondiferous kimberlites at Labiat and Chyulu, where lithospheric thickness has been determined from fitting theoretical geotherms to P-T estimates from nodule compositions. The grey diamond is the location of the diamondiferous kimberlite at Mwadui, where Cr/Ca array barometry gives a lower limit on the lithospheric thickness. Boxes are the locations of local earthquake studies as referred to in the text.

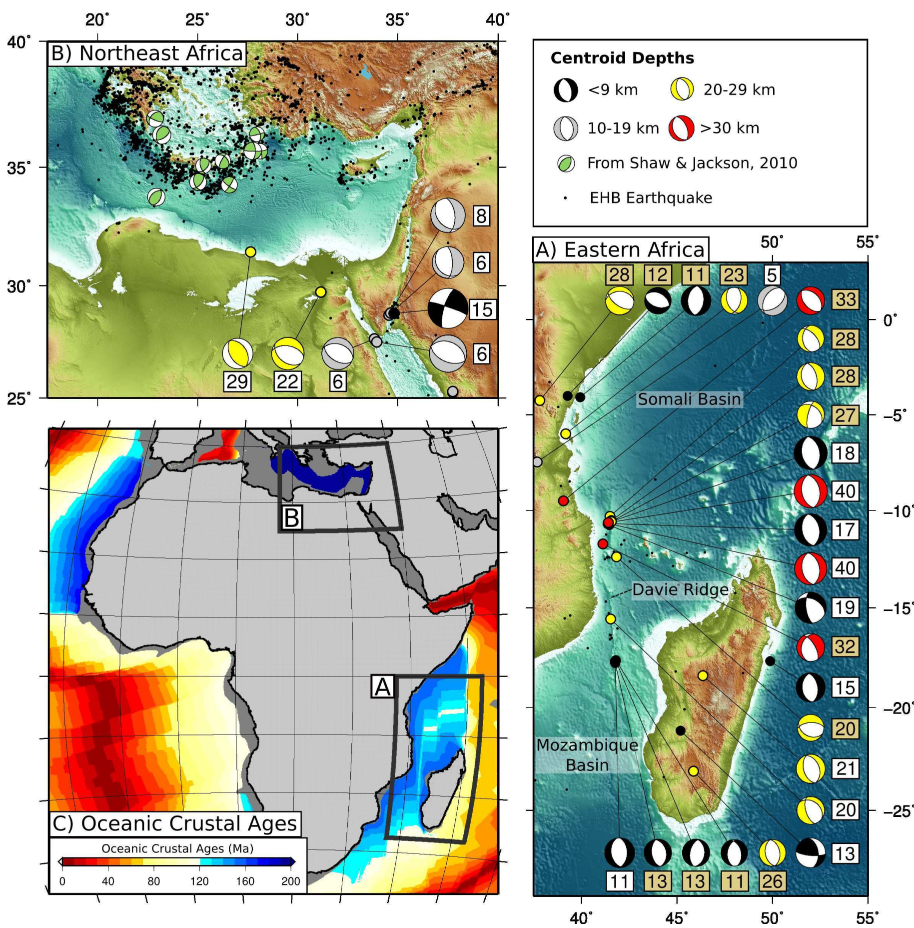

Figure 12: (a) East African margin. (b) Northeastern margin of Africa. Events in green are selected from Shaw and Jackson (2010), demonstrating faulting with trench-parallel P-axes, curving around with the trench axis. (c) Oceanic crustal ages, after Muller et al. (2008).

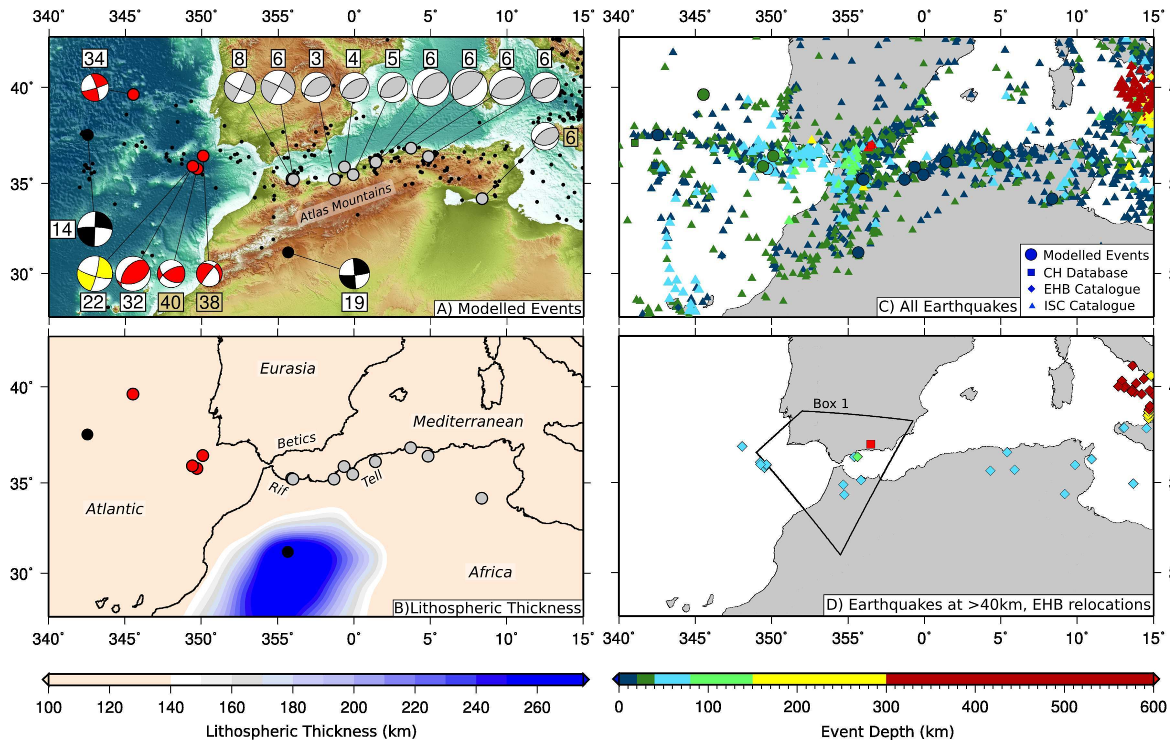

Figure 13: The Morocco/Algeria margin of northwest Africa. (a) Waveform modelling results. (b) Lithospheric thickness. (c) Full-catalogue seismicity of the western Mediterranean. (d) Earthquakes from the EHB and Centennial Hypocentre catalogues, with depths >40 km. Box 1 indicates the area within which Hatzfeld and Frogneux (1981) identified microearthquakes down to 150 km.

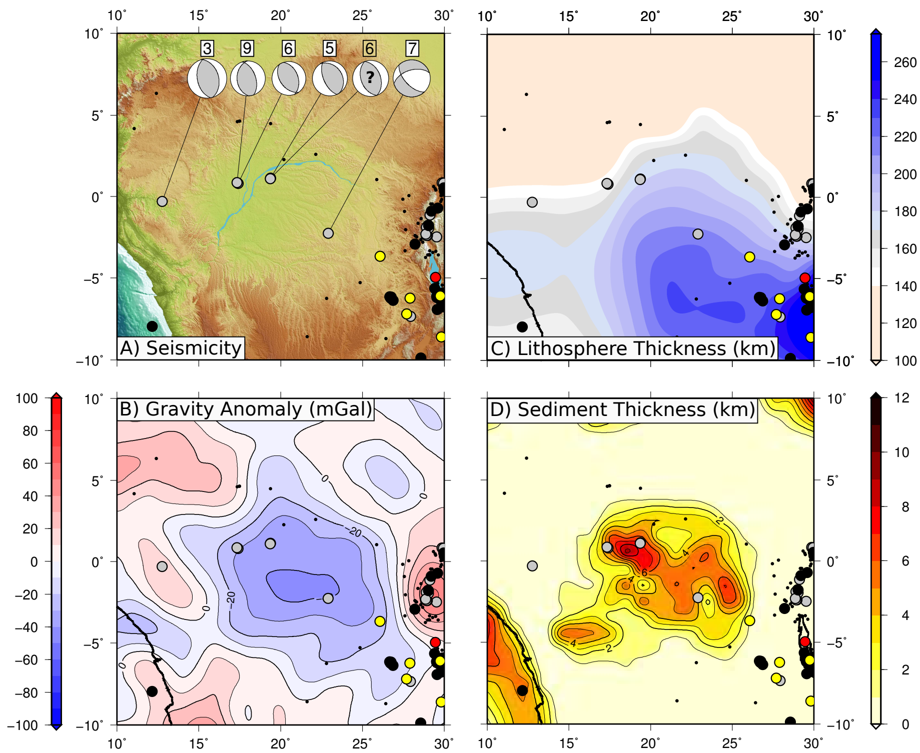

Figure 14: The Congo Basin. (a) Earthquake focal mechanisms and centroid depths from this study. No gCMT mechanism was available for the event marked by a **?**, so a mechanism consistent with available data was assumed for depth-phase modelling. Events on the EARS are shown in Figures 5,6. EHB catalogue earthquakes are shown as small black dots. (b) Free-air gravity anomalies over the Congo basin, with centroids indicated by colour of points for major earthquakes. (c) Lithospheric thickness across the Congo basin. The Congo basin formed within the extent of the Congo craton, associated with thick lithosphere. The effects of basin formation on the lithospheric thickness are considered by Crosby et al. (2010). (d) Sediment thickness, from Laske and Masters (1997).

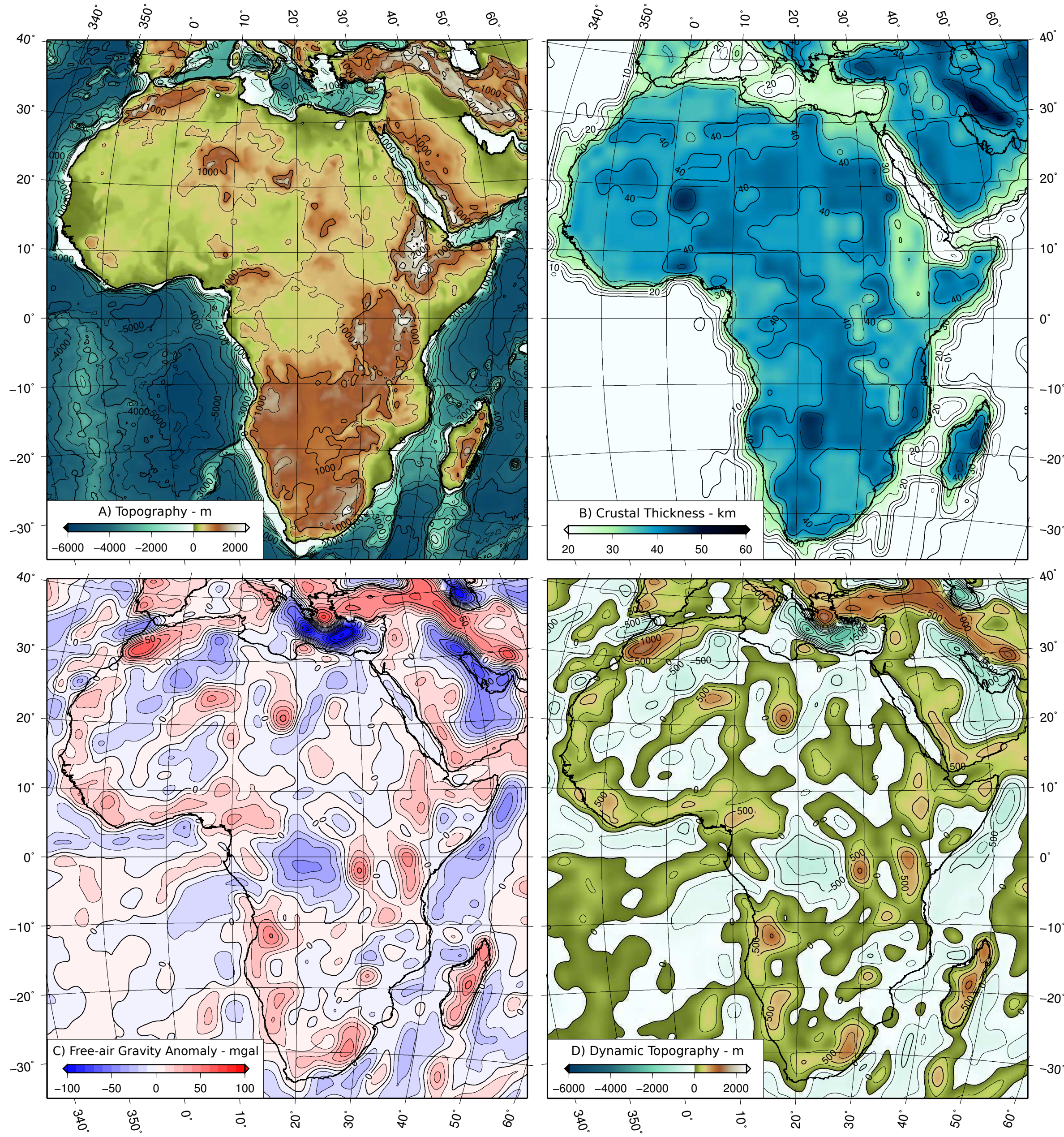

Figure 15: Data considered for dynamics calculations. (a) SRTM30PLUS topography, filtered to remove features at lengthscales of $\leq$ 100 km. (b) Crustal thickness from the CRUST2.0 model of Bassin et al. (2000). (c) Free-air gravity anomalies at $500 \leq \lambda \leq 4000$ km. (d) Dynamic topography, calculated from the free-air gravity anomaly using a mantle density of 3300 kg m^{-3}.

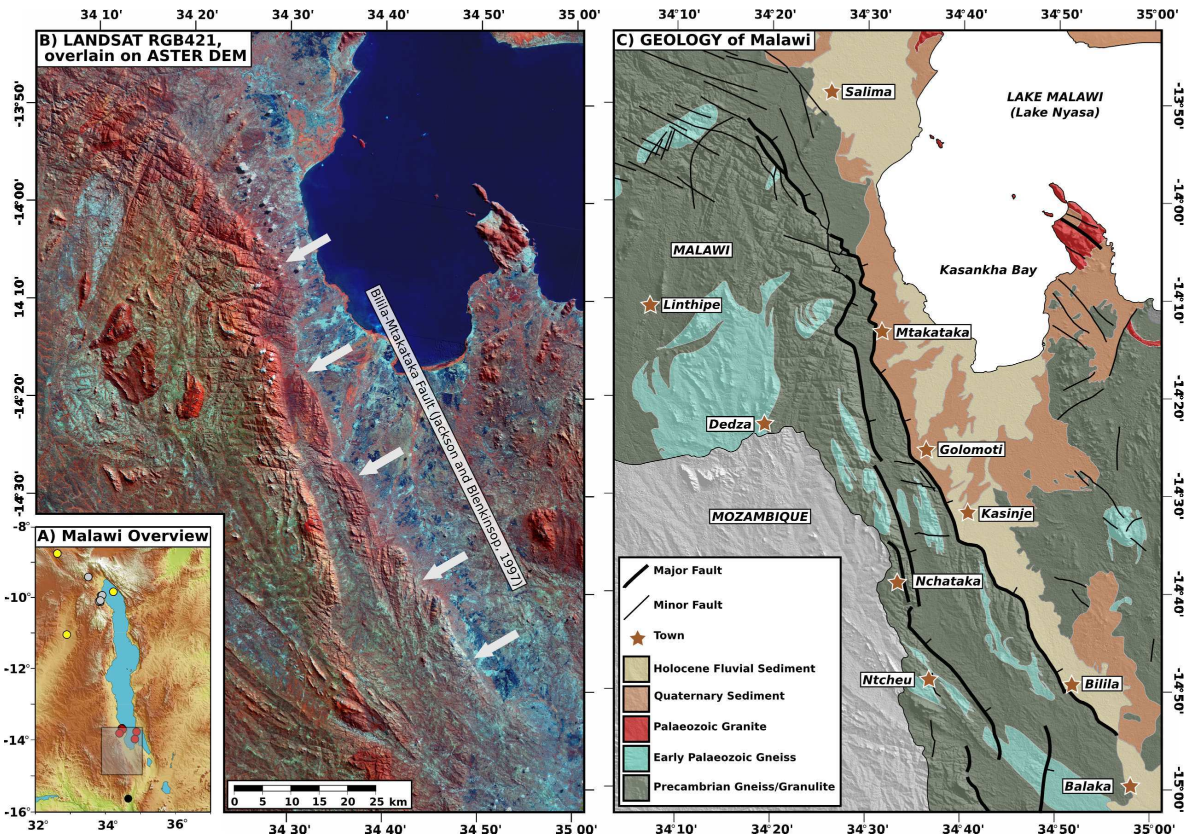

Figure 16: The Bilila-Mtakataka Fault, Southern Malawi. (a) Location map. (b) Landsat RGB 421 image, overlain on shaded ASTER DEM. Grey arrows indicate the Bilila-Mtakataka fault, as mapped by Jackson and Blenkinsop (1997), which ruptured in a single event. (c) Simplified geological map of the region, based on published maps from the Geological Survey of Malaŵi.

A Waveform modelling Results

Earthquakes modelled by body waveform inversion and used in this study. Results listed are from this study and taken from the literature.

Waveform modelling Results													
Date			Time		Lat/°	Long/°	Depth/km	M_W	Focal Mechanism			Reference	FPS
yyyy	mm	dd	hh	mm					Strike/°	dip/°	Rake/°		
1964	03	19	09	42	14.35	56.31	5	5.7	282	38	-119	H&S	
1964	05	07	05	45	-3.93	35.11	34	6.6	283	89	044	N&L	
1965	05	18	01	04	-17.69	49.87	15	5.4	350	50	-095	G&Ca	
1966	03	20	01	42	0.84	29.87	6	6.9	033	42	-100	F&J	
1966	05	06	02	36	-15.63	34.65	17	5.1	047	50	-124	S	
1966	05	17	07	03	0.82	29.94	6	5.8	003	53	-092	F&J	
1967	03	13	19	22	19.64	38.74	2	5.6	309	45	-100	H&S	
1968	05	15	07	51	-15.92	26.10	30	5.6	036	34	-113	F&J	
1968	12	02	02	33	-14.11	23.78	11	5.6	035	36	-081	F&J	
1969	02	28	02	40	35.92	-10.58	32*	7.6	070	44	113	G&Cb	
1969	02	28	02	40	35.92	-10.58	22*	7.7	014	82	-012	G&Cb	
1969	03	29	09	15	11.93	41.21	9	6.2	325	74	-020	F&J	
1969	03	31	07	15	27.52	33.94	6	6.6	294	37	-089	H&S	
1969	04	05	02	18	11.95	41.33	5	6.2	320	66	-051	F&J	
1969	04	22	22	34	12.76	58.23	10	5.2	350	63	-055	H&S	
1969	09	29	20	03	-33.19	19.32	5	6.3	305	87	003	F&J	
1972	06	28	09	49	27.65	33.82	6	5.7	288	40	-100	H&S	
1974	09	23	19	28	-0.30	12.76	3	6.0	344	41	086	F&J	
1975	04	04	17	41	-21.15	45.19	13	5.6	095	75	043	G&Ca	
1976	07	01	11	24	-29.56	25.11	8	5.7	126	64	-077	F&J	
1976	09	19	14	59	-11.05	32.90	29	5.6	349	42	-123	F&J	
1977	07	06	08	48	-6.20	29.54	14	5.3	348	63	-103	S	
1977	12	15	23	20	-4.76	34.98	12	5.4	168	56	-051	S	
1980	01	01	16	42	38.73	-27.75	12*	7.0	330	82	005	G&Cb	
1980	01	01	16	42	38.73	-27.75	20*	6.6	280	82	050	G&Cb	
1980	10	10	12	25	36.14	1.41	6*	7.0	220	46	072	N	
1980	10	10	12	25	36.14	1.41	6*	7.0	230	20	091	N	
1981	11	18	09	17	-2.26	22.90	7	5.7	137	60	-044	F&J	
1982	12	13	09	12	14.68	44.23	6	5.8	272	67	-139	S&S	
1983	01	24	16	34	39.65	-14.47	34	6.0	342	80	-006	G&Cb	
1983	07	07	20	35	-7.35	27.94	6	5.8	224	42	-089	F&J	
1983	09	30	18	58	11.78	43.40	5	5.6	058	87	160	F&J	
1983	10	17	19	36	37.57	-17.46	14	6.5	272	80	180	G&Cb	
1983	12	22	04	11	11.86	-13.51	4	6.3	112	48	-110	F&J	
1984	01	11	18	40	-6.23	27.90	24	5.5	021	66	-164	F&J	
1984	08	25	20	37	-8.76	32.63	26	5.3	081	65	-123	F&J	
1985	05	14	13	25	-10.68	41.39	40*	6.0	350	45	-090	G&Ca	
1985	05	14	13	25	-10.68	41.39	17*	6.0	350	45	-090	G&Ca	
1985	05	14	18	11	-10.62	41.41	40*	6.2	350	45	-090	G&Ca	
1985	05	14	18	11	-10.62	41.41	18*	6.2	350	45	-090	G&Ca	
1986	06	29	21	48	-4.96	29.46	36	5.6	191	81	-072	N*ea*	
1987	10	25	16	46	5.49	36.83	14	6.1	177	57	-127	F&J	
1987	10	28	08	58	5.79	36.76	9	6.0	189	41	-090	F&J	
1989	02	09	23	48	-8.60	29.82	25	5.2	172	37	-105	Y&C.a	
1989	03	09	02	37	-13.68	34.47	31	5.5	149	34	-099	F&J	
1989	03	10	21	49	-13.71	34.49	32	6.1	154	34	-092	J&B	
1989	08	20	11	16	11.74	41.95	5	6.4	302	46	-076	B&N	
1989	08	20	11	17	11.97	41.94	4	6.2	298	31	-073	B&N	
1989	08	20	19	25	11.89	41.81	6	6.1	295	29	-083	B&N	

Waveform modelling Results - Continued from previous page

Date			Time		Lat/°	Long/°	Depth/km	M_W	Focal Mechanism			Reference	FPS
yyyy	mm	dd	hh	mm					Strike/°	dip/°	Rake/°		
1989	08	21	01	09	11.85	41.83	6	6.4	292	42	-095	B&N	
1989	08	21	05	03	11.95	41.77	7	6.0	288	36	-087	B&N	
1990	05	15	15	21	-3.13	35.84	8	5.5	359	39	-109	F&J	
1990	05	15	16	24	-3.07	35.92	8	5.7	075	41	-099	F&J	
1990	05	20	02	22	5.12	32.18	13	7.2	321	69	014	G*ea*	
1990	05	24	19	34	5.32	31.88	14	6.3	120	56	-059	G*ea*	
1990	05	25	00	42	5.45	31.87	22	5.3	175	50	-080	Y&C.a	
1990	07	09	15	11	5.43	31.68	11	6.5	092	72	-062	G*ea*	
1990	07	27	20	41	5.07	32.18	35	4.8	335	52	-120	Y&C.a	
1991	01	24	12	55	-13.16	23.16	28	4.9	229	49	-110	Y&C.a	
1991	04	21	23	12	-18.42	46.35	21	5.4	338	41	-095	F&J	
1991	10	09	17	22	1.84	31.22	13	5.5	270	74	-046	F&J	
1992	03	05	08	55	11.52	42.80	9	6.2	317	75	002	F&J	
1992	09	11	03	57	-6.15	26.66	14	6.3	204	47	-119	F&J	
1992	09	23	14	52	-6.17	26.74	8	5.6	045	39	-072	F&J	
1992	10	12	13	09	29.72	31.15	22	5.8	128	43	-069	F&J	
1992	10	30	10	43	31.20	-4.33	19	5.7	085	81	-179	*ts*	
1993	03	13	17	12	19.60	38.76	13	5.6	075	62	146	*ts*	
1993	03	16	22	59	11.61	41.96	8	5.6	314	46	-071	F&J	
1993	04	11	19	41	-3.87	35.70	25	5.2	310	49	-085	Y&C.a	
1993	08	01	00	20	15.40	31.70	12	5.5	176	64	-024	*ts*	
1993	08	03	12	43	28.71	34.55	8	6.1	139	38	-119	F&J	
1993	08	03	16	33	28.79	34.64	6	5.6	143	27	-122	F&J	
1993	09	21	19	11	11.48	39.62	7	5.6	019	42	-097	F&J	
1994	02	05	23	34	0.56	30.08	17	6.0	187	31	-073	F&J	
1994	04	11	11	20	11.66	42.87	7	5.9	318	78	-020	*ts*	
1994	04	24	02	57	11.57	43.00	4	5.5	127	36	-071	*ts*	
1994	04	24	09	52	-9.05	30.47	32	5.1	340	61	-100	Y&C.a	
1994	05	26	08	26	35.25	-4.09	8	5.9	117	81	-175	B*ea*.a	
1994	08	18	00	45	-7.50	31.75	27	5.9	306	32	-101	F&J	
1994	08	18	01	13	35.47	-0.08	5	5.7	058	45	095	B&B	
1995	07	22	13	31	-13.98	34.84	33	4.9	315	50	-105	Y&C.a	
1995	08	10	00	41	-15.57	41.53	20	5.2	308	34	-120	*ts*	
1995	09	22	08	51	1.09	19.36	5	5.3	327	29	082	*ts*	
1995	09	30	20	46	-13.82	34.40	30	4.7	140	38	-075	Y&C.a	
1995	11	12	19	00	-13.76	31.61	29	4.8	220	52	-063	Y&C.a	
1995	11	22	04	15	28.78	34.81	15	7.1	197	73	-006	F&J	
1995	12	11	17	54	-6.23	26.72	8	5.4	227	45	-074	*ts*	
1997	03	09	17	40	11.64	43.49	7	5.7	068	41	-116	*ts*	
1997	09	21	18	13	-7.39	30.33	29	5.8	181	59	-071	F&J	
1998	03	05	02	59	0.80	17.40	6	5.2	145	46	079	*ts*	
1998	03	28	21	59	-6.14	29.52	14	5.2	227	69	033	*ts*	
1998	04	26	14	16	0.86	17.34	9	5.3	341	54	080	*ts*	
1998	05	28	18	33	31.44	27.65	29	5.5	148	49	090	*ts*	
1998	08	24	12	12	-13.77	34.89	44	4.7	335	53	-095	Y&C.a	
1998	10	01	19	17	14.40	53.73	8	5.6	294	80	-010	*ts*	
1999	05	07	02	10	-7.61	31.58	27	5.2	306	42	-101	Y&C.a	
1999	05	07	14	07	-7.51	31.71	26	5.3	323	37	-083	*ts*	
1999	12	22	17	36	35.21	-1.31	3	5.7	074	45	108	*ts*	
2000	03	02	02	44	-2.93	28.20	15	5.4	184	47	-060	Y&C.a	
2000	07	10	17	48	-7.21	27.69	21	4.8	220	60	-135	Y&C.a	
2000	10	02	02	25	-7.96	30.81	39	6.4	178	34	-077	*ts*	
2000	11	10	20	10	36.44	4.84	6	5.7	052	44	083	*ts*	
2001	05	25	22	18	17.96	40.00	4	5.3	326	48	-090	*ts*	

Waveform modelling Results - Continued from previous page

Date yyyy	mm	dd	Time hh	mm	Lat/°	Long/°	Depth/km	M_W	Focal Mechanism Strike/°	dip/°	Rake/°	Reference	FPS
2001	06	15	16	19	13.87	51.67	11	5.9	112	89	-001	*ts*	
2001	08	26	14	11	14.22	51.75	8	5.6	113	85	-005	*ts*	
2002	02	20	19	07	-7.67	31.96	37	5.4	231	32	-121	*ts*	
2002	05	18	15	15	-2.98	33.72	5	5.5	147	86	013	*ts*	
2002	08	09	22	08	11.83	43.60	4	5.2	314	42	-065	*ts*	
2002	08	10	15	56	13.55	39.79	10	5.6	136	27	-096	*ts*	
2002	08	31	22	52	-9.84	34.23	20	5.0	128	48	-126	B*ea*.b	
2002	09	01	17	14	14.26	51.91	9	5.9	116	89	014	*ts*	
2002	10	24	06	08	-1.96	29.04	8	6.2	209	47	-082	*ts*	
2002	10	24	07	12	-1.89	28.90	3	5.5	210	42	-075	Y&C.a	
2003	05	21	18	44	36.88	3.70	6	6.8	070	40	095	D*ea*	
2003	05	24	01	46	14.41	53.75	9	5.8	113	89	003	*ts*	
2004	02	24	02	27	35.21	-3.99	6	6.4	298	83	179	B*ea*.a	
2004	03	18	20	37	2.04	31.39	33	4.7	295	40	-080	Y&C.a	
2004	10	22	12	00	14.12	40.24	6	5.5	205	50	-065	*ts*	
2005	08	26	18	16	14.43	52.32	4	6.1	026	69	-168	*ts*	
2005	09	20	21	23	12.65	40.44	6	5.4	079	78	009	*ts*	
2005	09	24	19	24	12.44	40.54	5	5.6	296	83	144	*ts*	
2005	12	05	12	19	-6.28	29.73	16	6.6	142	52	-138	*ts*	
2005	12	06	05	53	-6.09	29.60	18	5.2	019	43	-072	*ts*	
2005	12	09	23	30	-6.15	29.67	11	5.5	055	53	-051	*ts*	
2006	01	09	21	00	-6.10	29.74	27	5.3	210	51	-032	Y&C.a	
2006	02	06	18	50	-9.88	28.56	18	4.9	208	50	-125	Y&C.a	
2006	02	22	22	19	-21.30	33.61	16	6.9	160	72	-071	*ts*	
2006	03	15	14	19	-21.10	33.63	9	5.6	173	72	-054	*ts*	
2006	09	24	05	59	-17.78	41.77	11	5.6	000	48	-083	*ts*	
2006	11	20	20	16	-21.13	33.11	7	5.1	170	50	-091	Y&C.a	
2006	12	30	08	30	13.31	51.32	9	6.5	109	86	030	*ts*	
2007	02	19	02	33	1.75	30.73	22	5.5	158	67	-157	*ts*	
2007	03	28	21	17	-6.24	29.66	9	5.7	099	90	-111	*ts*	
2007	06	15	18	49	1.75	30.79	22	5.8	165	68	-142	*ts*	
2007	07	15	20	42	-2.85	36.16	5	5.4	258	59	-083	*ts*	
2007	07	17	14	10	-2.82	36.38	9	5.9	062	37	-092	*ts*	
2007	08	02	13	37	12.48	47.40	7	5.7	223	78	-159	*ts*	
2007	08	18	07	44	-2.84	36.17	8	5.4	262	60	-070	*ts*	
2007	08	20	02	56	-2.74	36.25	5	5.5	217	43	-099	*ts*	
2007	12	08	19	55	-7.47	37.69	5	5.6	056	48	-073	*ts*	
2008	02	03	07	34	-2.31	28.86	9	6.0	161	37	-107	*ts*	
2008	06	06	20	02	35.88†	-0.66†	4	5.6	056	35	089	*ts*	
2008	08	27	06	46	-10.75†	41.47†	19	5.8	295	41	-140	*ts*	
2009	05	19	17	35	25.29†	37.74†	3	5.7	144	45	-093	*ts*	
2009	09	26	13	26	-7.53†	30.45†	23	5.1	352	38	-105	*ts*	
2009	11	05	07	12	12.11†	45.91†	4	5.6	096	58	-095	*ts*	
2009	11	14	04	50	-6.78†	29.82†	13	5.4	000	37	-109	*ts*	
2009	12	06	17	36	-10.13†	33.85†	6	5.7	346	52	-091	B*ea*.b	
2009	12	08	03	08	-9.95†	33.88†	6	5.8	019	54	-070	B*ea*.b	
2009	12	12	02	17	-9.94†	33.91†	4	5.5	341	53	-095	B*ea*.b	
2009	12	19	23	19	-10.11†	33.82†	5	5.9	347	45	-077	B*ea*.b	

Date			Time		Lat/°	Long/°	Depth/km	M_W	Focal Mechanism			Reference	FPS
yyyy	mm	dd	hh	mm					Strike/°	dip/°	Rake/°		

Table 1: Waveform modelling results across Africa. Date and Time are taken from the gCMT catalogue (Dziewonski et al., 1981). Locations are taken from the updated catalogue of Engdahl et al. (1998), except those indicated by † which are from the NEIC catalogue. Depth, moment and mechanism parameters are determined from waveform modelling. * indicates a double source event solution. The final column refers to the work in which the modelling results are published: H&S - Huang and Solomon (1987), G&Ca - Grimison and Chen (1988a), G&Cb - Grimison and Chen (1988b), N - Nábělek (1984b), S - Shudofsky (1985), Braunmiller and Nábêlek (1990), G*ea* - Gaulon et al. (1992), J&B - Jackson and Blenkinsop (1993), S&S - Seno and Saito (1994), N&L - Nyblade and Langston (1995), N*ea* - Nyblade et al. (1996b), F&J - Foster and Jackson (1998), B&B - Bezzeghoud and Buforn (1999), D*ea* - Deloius et al. (2004), B*ea*.a - Biggs et al. (2006), B*ea*.b - Biggs et al. (2010), Y&C.a - Yang and Chen (2010), *ts* - This study.

B Depth Phase Analysis Results

Earthquakes modelled with depth-phase analysis and used in this study. Results listed are from this study and taken from the literature.

Depth Phase Results

Date			Time		Lat/°	Long/°	Depth/km	M_W	gCMT Mechanism			Reference	FPS
yyyy	mm	dd	hh	mm					Strike/°	dip/°	Rake/°		
1983	05	09	16	15	-4.25	37.83	28	5.3	270	35	-120	N&L	
1986	03	14	04	16	-10.75	27.67	34	5.3	208	33	-105	N&L	
1990	03	13	23	05	-4.09	39.94	11	5.5	006⋆	47⋆	−088⋆	*ts*	
1990	09	07	00	12	5.46	31.66	16	5.5	044	43	-147	*ts*	
1991	03	29	09	06	5.19	32.68	17	5.2	106⋆	41⋆	−089⋆	*ts*	
1991	07	24	13	54	-18.32	34.85	33	5.0	209⋆	51⋆	−125⋆	*ts*	
1992	06	12	19	16	34.18	8.37	6	5.2	082	36	114	*ts*	
1992	11	14	05	54	-23.11	45.87	26	5.0	350	45	-090	*ts*	
1993	01	08	17	31	12.96	49.37	15	5.5	070•	45•	−090•	*ts*	
1994	07	20	11	32	-4.25	35.59	21	4.5	301	64	-011	B*ea*	
1994	08	17	03	23	-4.48	35.59	15	3.7	335	35	-010	B*ea*	
1994	09	05	04	08	-7.50	31.70	15	4.1	318	36	-063	B*ea*	
1994	09	30	01	36	-5.92	29.89	11	4.5	335	36	-010	B*ea*	
1994	11	12	12	17	-6.94	29.55	18	5.3	204	80	-020	B*ea*	
1994	11	12	20	16	-6.65	30.14	8	4.7	303	46	-035	B*ea*	
1994	11	16	01	08	-9.42	33.51	7	4.5	301	64	-011	B*ea*	
1994	11	27	04	20	-4.08	35.83	11	4.0	093	69	-022	B*ea*	
1994	12	25	04	25	-5.17	30.58	29	4.2	215	55	-065	B*ea*	
1995	01	29	00	23	-5.03	35.92	9	4.1	162	43	-071	B*ea*	
1995	02	12	16	37	-3.88	35.67	34	4.5	316	68	-077	B*ea*	
1995	09	25	17	04	1.13	19.38	6	5.5	340•	45•	090•	*ts*	
1996	03	24	08	24	0.53	29.96	10	5.3	179	24	-094	*ts*	
2001	06	29	23	40	0.20	30.03	19	5.2	017	33	-060	*ts*	
2001	10	19	13	01	-7.96	12.15	12	5.4	160•	45•	090•	*ts*	
2002	01	20	00	14	-1.78	29.03	10	5.1	039	49	-042	*ts*	
2002	01	21	04	39	-1.77	29.00	9	5.0	055•	65•	−100•	*ts*	
2002	03	05	17	07	-11.84	24.90	18	5.1	230•	45•	−090•	*ts*	
2002	07	16	14	50	-11.73	41.13	32	5.2	195	34	-050	*ts*	
2002	11	04	03	19	-5.63	36.02	15	5.5	000•	45•	−090•	*ts*	
2003	03	20	06	15	-2.48	29.52	7	5.2	017	45	-023	*ts*	
2003	04	10	16	03	-5.65	29.40	13	5.1	061	46	-049	*ts*	
2003	06	14	03	10	-5.64	36.04	10	5.0	340	26	-112	*ts*	
2003	08	05	18	56	-0.71	29.59	13	5.2	330	34	-155	*ts*	
2005	01	04	19	58	-10.31	41.49	28	5.0	177	39	-058	Y&C.a	
2005	01	15	05	13	-6.00	39.18	23	5.0	159	45	-116	*ts*	
2005	09	24	06	58	12.57	40.48	6	5.3	173	39	-068	*ts*	
2005	09	28	16	31	12.41	40.57	3	5.1	341	36	-074	*ts*	
2006	02	23	01	23	-21.39	33.43	11	5.8	172	51	-090	Y&C.b	
2006	02	23	02	22	-21.42	33.49	19	5.3	190	51	-070	Y&C.b	
2006	03	15	11	52	-21.11	33.53	8	5.1	182	60	-048	Y&C.b	
2006	03	22	11	35	-21.36	33.23	12	5.2	017	42	-059	*ts*	
2006	04	10	13	36	14.50	39.95	4	4.9	172•	29•	−075•	*ts*	
2006	04	14	18	41	-21.36	33.69	19	5.2	022	37	-061	*ts*	
2006	04	27	04	18	0.35	30.00	15	5.2	189	32	-086	*ts*	
2006	05	12	18	13	-21.29	33.45	20	4.8	142	42	-104	Y&C.a	
2006	05	29	15	30	0.36	30.06	16	4.9	180	51	-135	*ts*	
2006	06	25	04	51	-17.64	41.80	11	4.9	188	46	-074	*ts*	
2006	06	30	01	07	-21.13	33.27	4	5.0	170	45	-106	*ts*	
2006	07	13	05	36	-8.36	30.32	31	4.8	162	34	-098	Y&C.a	

Depth Phase Results - Continued from previous page

Date yyyy	mm	dd	Time hh	mm	Lat/°	Long/°	Depth/km	M_W	gCMT Mechanism Strike/°	dip/°	Rake/°	Reference	FPS
2006	08	23	00	53	-21.32	33.32	18	5.0	352	40	-089	*ts*	
2006	09	17	07	30	-17.68	41.80	13	5.1	003	37	-096	*ts*	
2006	09	17	13	24	-17.70	41.75	13	5.1	347	38	-095	*ts*	
2007	02	12	10	35	35.78	-10.29	40	6.0	125	49	146	*ts*	
2007	06	18	23	51	-12.40	41.84	20	5.0	116	36	-066	*ts*	
2007	07	15	11	24	-2.92	36.20	7	5.3	235	47	-124	*ts*	
2007	07	26	18	54	-2.67	36.05	6	5.2	233	45	-116	*ts*	
2007	08	18	07	44	-2.84	36.17	10	5.2	260	45	-082	*ts*	
2007	09	08	14	15	-2.62	36.12	6	4.9	213	36	-092	*ts*	
2007	12	23	12	56	-4.01	39.28	12	4.9	299	42	-082	*ts*	
2007	12	23	13	45	-2.80	36.20	9	5.2	106	36	-100	*ts*	
2008	01	21	02	49	-10.53†	41.56†	28	5.2	165	34	-090	*ts*	
2008	01	21	15	28	-10.57†	41.57†	27	5.1	308	36	-151	*ts*	
2008	02	03	10	56	-2.40†	28.97†	9	5.0	010	42	-068	*ts*	
2008	02	03	11	12	-21.32†	33.09†	7	5.1	187	45	-069	*ts*	
2008	02	14	02	07	-2.40†	28.92†	8	5.3	005	45	-084	*ts*	
2008	04	20	07	30	-3.67†	26.07†	26	5.2	207	75	-180	*ts*	
2008	04	29	01	27	11.72†	42.81†	7	5.0	309	47	-056	*ts*	
2008	10	05	00	02	-1.13†	29.12†	9	5.3	347	41	-131	*ts*	
2008	11	13	11	07	-6.37†	26.86†	10	5.0	031	40	-087	*ts*	
2008	12	14	09	43	-7.35†	30.13†	23	5.2	322	15	-115	*ts*	
2009	05	19	19	57	25.24†	37.74†	4	4.8	330	46	-064	*ts*	
2009	12	11	04	49	-10.09†	33.86†	8	4.9	320	42	-096	*ts*	
2009	12	17	01	37	36.46†	-9.90†	38	5.6	316	35	-170	*ts*	
2010	01	28	23	52	-0.90†	29.20†	14	4.9	015	43	-080	*ts*	
2010	08	03	19	42	-9.50†	39.06†	33	5.2	313•	41•	−096•	*ts*	
2010	10	23	11	08	4.71†	35.79†	16	4.8	030•	45•	−090•	*ts*	

Table 2: Depth Phase results across Africa. Date, Time, magnitude and mechanism parameters are taken from the gCMT catalogue (Dziewonski et al., 1981). Locations are taken from the updated catalogue of Engdahl et al. (1998). Locations marked with † are taken from the NEIC catalogue. For events from the study of Brazier et al. (2005), mechanism parameters and depth are determined through regional, rather than teleseismic, studies, and locations are taken from the ISC catalogue. Events marked ⋆ have mechanisms taken from Foster and Jackson (1998), but with re-determined depths. Events marked • are not included in the gCMT catalogue, so no mechanism was available. For the purposes of forward modelling, a mechanism similar to the regional average is assumed - on figures, these mechanisms are marked with a "**?**". The final column refers to the work in which the modelling results are published: N&L - Nyblade and Langston (1995), B*ea* - Brazier et al. (2005), Y&C.b - Yang and Chen (2008), Y&C.a - Yang and Chen (2010), *ts* - This study.